DISSERTATIONES
CHIMICAE
UNIVERSITATIS
TARTUENSIS
152

CAROLIN SIIMENSON

Electrochemical characterization of halide ions adsorption from ionic liquid mixtures at Bi(111) and pyrolytic graphite electrode surface

DISSERTATION CHIMICAE UNIVERSITAS TARTUENSIS
152

CAROLIN SIIMENSON

Electrochemical characterization of halide ions adsorption from ionic liquid mixtures at Bi(111) and pyrolytic graphite electrode surface

UNIVERSITY OF TARTU
Press

Institute of Chemistry, Faculty of Science and Technology, University of Tartu, Estonia

Dissertation is accepted for commencement of the degree of Doctor of Philosophy in Chemistry on June 30th, 2016 by Council of Institute of Chemistry, University of Tartu

Supervisors: PhD Liis Siinor
Prof. Enn Lust
Department of Chemistry, University of Tartu, Estonia

Opponent: Prof. Claudine Buess Herman
Department of Chemistry, Université Libre de Bruxelles, Belgium

Commencement: August 11th, 2016, at 10:00
Ravila Street 14a, Tartu (Chemicum), auditorium 1021

ISSN 1406-0299
ISBN 978-9949-77-147-9 (print)
ISBN 978-9949-77-148-6 (pdf)

University of Tartu Press
www.tyk.ee

TABLE OF CONTENTS

1. LIST OF ORIGINAL PUBLICATIONS

I. **C. Siimenson**, L. Siinor, K. Lust, E. Lust, The electrochemical characteristics of the mixture of 1-ethyl-3-methylimidazolium tetrafluoroborate and 1-ethyl-3-methylimidazolium iodide. Journal of Electroanalytical Chemistry, 730 (2014) 59–64.

II. **C. Siimenson**, L. Siinor, K. Lust, E. Lust, Electrochemical Characterization of Iodide Ions Adsorption Kinetics at Bi(111) Electrode from Three-Component Ionic Liquids Mixtures. ECS Electrochemistry Letters, 4 (2015) H62–H65

III. L. Siinor, J. Poom, **C. Siimenson**, K. Lust, E. Lust, Electrochemical characteristics pyrolytic graphite | mixture of 1-ethyl-3-methylimidazolium tetrafluoroborate and 1-ethyl-3-methylimidazolium iodide interface. Journal of Electroanalytical Chemistry, 719 (2014) 133–137.

IV. **C. Siimenson**, M. Lembinen, O. Oll, L. Läll, M. Tarkanovskaja, V. Ivaništšev, L. Siinor,. T. Thomberg, K. Lust, E. Lust, Electrochemical investigation of 1-ethyl-3-methylimidazolium bromide and tetrafluoroborate mixture at Bi(111) electrode interface. Joural of The Electochemical Society, 163 (2016) H723-H730

Author's contribution:

Paper I: Performed all electrochemical measurements, modelling of data and interpretation of results.

Paper II: Performed all electrochemical measurements and interpretation of results.

Paper III: Performed electrochemical measurements and interpretation of results.

Paper IV: Performed all electrochemical measurements, modelling of data and interpretation of results.

2. ABBREVATIONS AND SYMBOLS

A	–	electrode area
AFM	–	atomic force microscopy
ARPES	–	angel-resolved photoemission spectroscopy
CE	–	counter electrode
CPE	–	constant phase element
C	–	capacitance
C_c	–	concentration
C_{ad}	–	adsorption capacitance
C_{dl}	–	double layer capacitance
CV	–	cyclic voltammetry
D	–	diffusion coefficient
DFT	–	density functional theory
EDL	–	electrical double layer
EDLC	–	electrical double layer capacitor
EIS	–	electrochemical impedance spectroscopy
Et_4NBF_4	–	tetraethylammonium tetrafluoroborate
$EMImBF_4$	–	1-ethyl-3-methylimidazolium tetrafluoroborate
EMImI	–	1-ethyl-3-methylimidazolium iodide
EMImOTF	–	1-ethyl-3-methylimidazolium trifluoromethanesulfonate
EMImCl	–	1-ethyl-3-methylimidazolium chloride
EMImBr	–	1-ethyl-3-methylimidazolium bromide
$EMImPF_6$	–	1-ethyl-3-methylimidazolium hexafluorophosphate
EMIm TFSI	–	1-ethyl-3-methylimidazolium bis(trifluorometylsulfonyl)imide
EQCM	–	electrochemical quartz crystal microbalance
ϕ	–	impedance phase
fcc	–	face-centered cubic crystal structure
Γ	–	surface excess
GCh	–	Gouy-Chapman theory
GCS	–	Gouy-Chapman-Stern model
HOPG	–	highly oriented pyrolytic graphite
HSC	–	hybrid supercapacitor
I_0	–	current amplitude
i_p	–	peak current
IL	–	ionic liquid
j	–	imaginary unit
j	–	current density
n	–	number of electrons
NTf_2	–	bis(trifluoromethyl sulfonyl)amide
ρ	–	density
PC	–	propylene carbonate
PG	–	pyrolytic graphite

$PMImPF_6$	–	1-propyl-3-methylimidazolium hexafluorophosphate
pzc	–	potential zero charge
R_{ct}	–	charge transfer resistance
R_D	–	diffusion resistance
R_{el}	–	electrolyte resistance
RE	–	reference electrode
R_{sol}	–	solution resistance
RTIL	–	room temperature ionic liquid
SC	–	supercapacitor
STM	–	scanning tunneling microscopy
t	–	time
v	–	potential scan rate
ΔV	–	voltage range
VOC	–	volatile organic compound
Z	–	complex notation of impedance
Z_0	–	magnitude of impedance
Z'	–	real part of impedance
Z''	–	imaginary part of impedance
ω	–	angular frequency
WE	–	working electrode
δ	–	phase angle

3. INTRODUCTION

Surface active anions are involved in many technological processes influencing the structure and 2D layer formation for corrosion inhibitors, catalysts activatiors, etc. Therefore, the adsorption of halide ions has been studied by electrochemist for a long time from aqueous solution and from classical organic electrolytes. However, since ionic liquids (IL) have shown high potential in modern electrochemical devices, the characterization of the interface between electrode and IL is the first priority of interfacial electrochemists.

Halides are attractive ions for electrolyte design, ensuring sometimes reversible redox reaction as well as increase in ionic conductivity. For the practical point of view, halides are cheap and ecologically friendly anions [1,2]. The future of electrochemistry lies on the design of complex interfaces and on future development of experimental electrochemical methods moving towards single molecule measurements. Predicting the properties of interfaces between metal|electrolyte using different computational methods have improved significantly in recent years. It allows to predict properties and interactions of a large variety of molecules or ions. However, experimental data is needed to confirm new models.

The main aim of this work was to investigate the influence of the addition of halide ions in room temperature ionic liquid (RTIL) medium for electrical double layer (EDL) parameters at Bi(111) single crystal electrode. For further characterization of electrochemical behavior of RTIL mixtures with iodide ions in a wider region of potentials pyrolytic graphite (PG) electrode was used. Influence of electrode potential and halide ion concentration in RTILs has been characterized by cyclic voltammetry (CV) and electrochemical impedance spectroscopy (EIS) methods. Bi(111)|RTIL mixtures were studied as a model system for the further investigation of these promising electrolyte mixtures for supercapacitors, actuators, electrochemical switches and others modern electrochemical energy storage devices. The data for Bi(111)|RTILs were compared to PG|RTIL interface as well as with two electrode capacitor system. Also *in situ* scanning tunneling microscopy (STM) and computational methods have been used for the detailed characterization of the electrode|RTIL interface.

4. LITERATURE OVERVIEW

4.1. General overview

Electrochemistry has not always been the science of interfaces, but nowadays the number of surface sensitive techniques and application is quickly increasing [3]. The future of electrochemistry lies mainly on the development of methods for detailed analysis of adsorption and charge transfer processes that take place at the interface. The understanding of complicated interfacial structure of metal and semiconductor electrodes, influence of the crystallographic structure and orientation of the surface, adsorption of different types of adsorbates helps to develop important applications such as protection against corrosion, electro-catalysis, sensors and modern electrochemical energy storage and recuperation devices. The importance of anion adsorption in electrochemistry is found on the principle that usually anions are less strongly solvated compared with cations. Therefore, anions are more often specifically adsorbed because their solvation sheaths are easier to break up at more positively charged metal and semi-conductor electrode surfaces. Anions like Cl^-, Br^- and I^- are the most extensively studied specifically adsorbing anions in electrochemistry [4–10]. The progress in development of the efficient methods for preparation of well-defined single crystal surfaces has paved the way for get better understanding of the role of anions in surface electrochemistry. Most widely used metal electrodes in electrochemistry are Au, Ag, Pt, Hg as well as Bi, Pd, Ir, Cd, Sb [11–14]. For metals with face-centered cubic (fcc) lattice the surface structure can be generated by cutting the lattice parallel to the sides of a cube that forms a unit cell. Electrochemical polishing and annealing have also showed good results for preparing the flat well-defined metal (Bi, Cd, Sb) surfaces for fundamental studies. In addition for Pt(hkl) group and Au(hkl) single crystal electrode the flame-treatment methods have been worked out and have been widely applied [5,15–20].

If water is an appropriate solvent for electrochemical application, it should be used without hesitation. However, if the other non-aqueous solvents are employed, there is always a question about environmental hazards. Under the framework of green chemistry various non-aqueous solvents, immobilized solvents, ionic liquids, supercritical fluids, aqueous and solvent-free reaction systems are studied as electrolytes for electrochemical devices [21]. Besides the environmental friendliness, the advantages of using aqueous electrolytes are high ionic conductivity (~0.8 S/cm for H_2SO_4), low sensitivity to moisture and oxygen as well as end of life disposal of devices. However, the use of non-aqueous electrolytes provides larger variety of electrolyte-solvent systems and many advantages. For example, in EDLCs containing aqueous electrolytes the charging potential (ΔV) is limited, varying usually from 1.0 to 1.5 V (e.g. H_2SO_4, Li_2SO_4, LiF, Na_2SO_4, NaF). For non-aqueous electrolytes cell potential up to 3.5-4.0 V have been obtained (from 0.5-1.0 M Et_4NBF_4 in PC), limited by the faradic breakdown of the electrolyte. The market for EDLCs with high

surface area carbon electrodes and aqueous electrolytes is about $150-$220 million annually. The remaining problems needed to unravel, compared with aqueous electrolytes, are higher specific resistance and cell operating time due to the decomposition of the electrolyte [21–23].

The advantage of using ILs as an electrolyte in EDLCs is the possibility that the system can be charged to wider potential region and therefore higher specific energy values can be obtained [24–26]. Ionic liquids are one of the materials that impact on a broad range of energy storage systems offering an opportunity to optimize the performance of electrolytes by choosing cations and anions as needed. ILs as electrolytes are used in high-energy-density and low cost batteries, dye-sensitized solar cells, thermo-electrochemical cells, electrical double layer capacitors and in CO_2 reduction devices [27,28]. Compared with aqueous and classical organic electrolytes, ILs are composed of ions, no solvent molecules or solvation sheaths. Due to this effect there is a lack of fundamental understanding for predicting and understanding the complicated interfacial structure of these electrolytes at electrode surface. Mainly experimental works has been carried out metal at electrodes as well as on glassy-carbon and well defined graphite electrodes in RTILs. Some theoretical and computational models have been developed by Kornyshev, Fedorov, Koper and others [9,14,29–38].

Over the last 10 years the sensitivity of surface analysis methods and techniques have improved significantly [39–41]. Nowadays, detailed characterization of the electrode|electrolyte interface can be carried out using multiple methods. Sometimes at the electrode interface the fast kinetic processes take place and due to that, the *in situ* measurements are preferred, starting with the classical electrochemical methods like cyclic voltammetry (CV) and electrochemical impedance spectroscopy (EIS) and moving on to the pulse potentiodynamic and galvanostatic methods that have been applied to study the adsorption of organic compounds at solid metals. Raman, *in situ* photoelectron spectroscopy (XPS), infrared (IR)and UV-vis spectroscopies have been used to identify adsorbed intermediates and the nature of chemisorption bonds. With different X-ray methods it is possible to get information about the coordination numbers of adsorbed spices and the substrate-adsorbate and adsorbate-adsorbate bond lengths. For the visualization of the electrode surface, structure of deposited adlayers and interface morphology, *in situ* STM and AFM methods can be used [42–44]. Due to the high cost, complicated and time consuming experiments on porous carbon electrodes, it is reasonable to use ILs and their mixtures in model single crystal metal electrode based systems to find and study new electrolytes with a good electrochemical stability in a wide range of potentials [45–47]. The implementation of ILs in EDLCs or hybrid supercapacitors (HSCs) as electrolytes could quadratically increase the energy and power density values as number of papers have shown [25,26,46,48–55].

4.2. Ionic liquids

Ionic liquids (ILs) can be defined as semi-organic fluid salts composed entirely of bulky asymmetric organic cations and organic or inorganic anions, with a melting temperature below the boiling point of water. In general, an IL differs from a traditional molten salt because they are made from organic cation and inorganic or organic anions (Figure 1). The history of ionic liquids goes back to the beginning of 20th century, when Paul Walden reported the physical properties of ethylammonium nitrate and with that a new class of liquids were discovered. As soon as air and water stable ILs were synthesized in the early 1990s, they have attracted the interest of a considerable part of the material science, electrochemical and organic chemistry community. Nowadays, ILs are starting to leave academic labs and find their way into a wide variety of industrial applications [56–58]. Despite the best efforts and technology applied for organic compounds handling an estimated 20 million ton of volatile organic compounds (VOCs) is released into the atmosphere each year as a result of industrial processing. Solvents compose 2/3 of all industrial emission and 1/3 of all VOC emissions. ILs can help to make the processes more efficient and environmental friendly. The most intriguing features of ILs for industrial aspects are essentially very low vapor pressure and incredibly large thermal stability up to 400 °C [59].

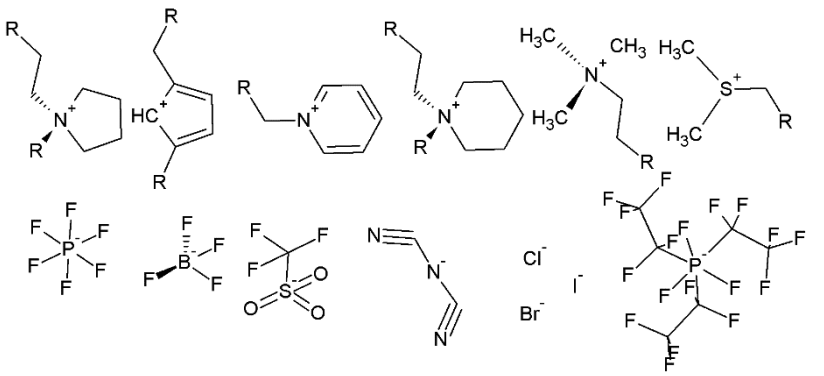

Figure 1. Examples of some commonly used IL systems [28].

4.2.1. General properties

The melting point of ILs depends on a balance between cation and anion symmetry, flexibility of chains in the ions, and charge accessibility. Increase of the length of alkyl chains in the cation and/or increase of the anion size generally lead to a decrease in the melting point. At atmospheric pressure some ILs stay in the liquid state up to temperatures as high as 200–300 °C, due to the strong ion-ion interactions. The thermal stability is determined by the strength of IL heteroatom-carbon and heteroatom-hydrogen bonds. For a short time

treatment high thermal stability values have been reported for several ILs. For example the 1,2-dimethyl-3-propyl imidazolium bis(trifluorosulfonyl)imide is stable up to 457 °C [60]. Not only the high thermal stability makes these salts so attractive, but also the low melting point. Many of them are liquids at room temperature. Therefore, in this work abbreviation IL is used for all ionic liquids and RTIL is used for these that are in liquid state below the room temperature. For some ILs the freezing and melting temperatures are reported as different values. When the IL is cooled its viscosity increases and the increased viscosity prevents formation of the first crystals. The liquid phase solidifies into an amorphous solid phase and this temperature is characterized as glass transition temperature. So, the temperature at which the solidification is observed may depend on the way of the cooling (Table 1) [28,36,61].

Table 1. Examples of melting and freezing temperatures of some ILs [28,62,63].

Ionic Liquid	Melting point (°C)	Observed temperature of solidification (°C)
$EMImBF_4$	11, 14.6, 15	−63
EMImI	79	39
EMImCl	89	33
EMImBr	79	30
$EMImPF_6$	62, 58	5
$PMImPF_6$	40, 21	−81

The main bottlenecks in the development of electrochemical devices based on ILs are high viscosity and low diffusion coefficient of ions. At room temperatures viscosity of ILs varies between 20 and 40 000 cP and conductivities are within a broad range of 0.1 to 18 mS/cm. Also it is quite complicated to predict the conductivity of IL under design, because in classical electrolyte solutions the conductivity depends on the number of charge carriers and is inversely proportional to the medium viscosity, density and solvation energy. However, in ILs the system consists entirely of charge carriers, but the conductivity values are lower compared with aqueous electrolyte solutions. The formation of different ionic species and aggregates may be expected due to the interaction of opposite charge ions and it is difficult to define the number of charge carriers. Generally, ILs are more viscous than common molecular solvents and the viscosity is determined by the van der Waals forces and hydrogen bonding. Also electrostatic forces and alkyl chain lengthening in the cation influence the viscosity [28,32,36,61].

ILs are denser than water. The density values are ranging from 1 to 1.6 g cm^{-3} and the density values decrease with increase in the length of the alkyl chain in the cation. The influence of cations composition on the density of the RTILs is less obvious compared to that provided by the nature of the anion.

The relation is likely effected by the ionic associations that a given cation exerts with an anion. Also the density is affected strongly by the identity of the anion. Comparing the experimental densities of the pyridinium-based and imidazolium-based ILs, the density value increases with the increase in the molecular weight for the anion. However, for some anions (and ILs), the density does not directly correspond to a rise in the molecular weight. This phenomenon can be explained by the strongly localized charge in the anions, which gives the possibility of a stronger ion pairing with the cation, resulting in a higher density [64]. For example, ILs containing BF_4^- anions usually have lower densities than PF_6^- or $CF_3SO_3^-$ based ones [32,64,65].

The charge transfer properties of ILs directly influence the electrochemical performance. For the electrochemical applications not only the EDL equilibrium properties are important, but also the dynamics of the charging-discharging. In the fundamental point of view, it is interesting that the measured electrical conductivity of many RTILs significantly deviates from the Nernst-Einstein relation [66]. Usually the Nernst-Einstein relation is used for the determination of ionic diffusion coefficients from conductivity measurements or for predicting conductivities by using models of ionic diffusion. This phenomenon is explained by the smaller degree of ion pair dissociation. Typically, the degree of ion pair dissociation varies between 50 to 70%. Also experimental results show that small anions have reduced mobility compared to cations (usually much larger) and this is explained by the stronger interactions, so-called solvation of the anions by the counter ions. The main factor that determines the magnitude of self-diffusion for imidazolium based ILs are the ion size, the geometric shape and the charge localization/delocalization of the anion. The diffusion of ions is also controlled by the shape and size of ions, the strength of interactions between cation and anion, conformational flexibility, molecular mass of ions. The solvent additives strongly influence the viscosity and conductivity, and the effects of formation of local nanostructures is also important [36,65,67,68].

4.2.2. Electrochemical properties

For the electrochemical applications ILs can provide exiting properties and opportunities for overcoming problems and limitations encountered in traditional chemical processes. Most conventional solvents (e.g. water) suffer from the drawback that it has a relatively narrow region of ideal polarizability, so-called potential window. For example, ILs based on NTf_2^-, BF_4^- and PF_6^- anions, are stable in some cases to below Li/Li^+ reduction region [69]. The electrochemical reactions in principle are the processes at the electrode|IL interface, including the diffusion of electroactive species, capacitance of the interface, rate of electron transfer processes, etc., and which will dominate the performance in the electro-chemical applications of ILs. The understanding of the surface electrochemistry in ILs will benefit the performance enhancement of their applications. Most of the electroanalytical methods and electrochemical sensors are based on the

change in electrochemical properties at the electrode|electrolyte interface. Reactions that take place at the interface between metal electrode and solutions are important in the metal deposition, corrosion, film formation, electro-organic synthesis, etc. For the better control of these processes a detailed knowledge of the properties of the electrode|IL interface is needed. The stability of the charged electrode|IL interface is of great importance because in many modern applications there is a strong need for ILs that are electrochemically stable within a wide range of potentials. Since the electrochemical stability of the pure ILs depends on the electrochemical stability of the cation and/or anion, understanding the ion behavior at the electrode interface leads to improvement and implementation of the ILs to the desired system. Some common ILs are stable up to 5–6 V [70], however typically 2–3 V. This is much higher than for aqueous electrolytes. Naturally, the stability of electrolyte depends strongly on the type of electrodes used. The most popular metallic electrodes are Au, Hg, and Pt due to their high stability in wide range of potentials. Recently, the interest in the properties of carbon|IL interface (based on glassy carbon, graphite, carbide derived carbon, etc. electrodes) has been developed for the potential use of these materials [28,36,56]. Starting a new investigation of an IL or choosing an IL for experiment, first information for cathodic and anodic stability can be obtained from the literature. Thereafter cyclic voltammetry method (discussed below) can be used for determination of the stability of the IL system under study. The big variation of the stability limits of ILs in the literature is caused by the residual water and mostly by the halide anions contamination. Halides can undergo anodic oxidation at relatively low positive potentials and according to this, the potential region, where the IL is electrochemically stable, is narrower [28,36,44].

4.3. Bismuth

A number of studies by Costa et al. [14,30], Lust et al. [15,71,72] and many other experimental and computational data highlight the importance of the electrode material have been carried out [53,73–79]. Thus, the choice of the electrode material for the investigation of electrode|electrolyte interface is decisive. Bismuth is a semi-metal with atomic number 83. In the literature Bi is described as “mercury-like” element as well as similar to cadmium and antimony. However, mercury was a widely used electrode material in analytical electro-chemistry, but the toxicity of the mercury is still a problem, therefore alternative and more environmental friendly electrode materials are highly desired for different applications. Bi surface represents also properties characteristic to quasi–two–dimensional metals (with unique spin properties), which can be used in a novel type of electronics by creating a much higher speed spintronic devices and especially with very low power (because of the reduced Ohmic losses) [15,80,81].

In recent years there has been a growing interest for the application of Bi as an electrode material for sensors, detectors, etc., from both experimental and theoretical point of view. Considerable progress has been made for the describing the geometric and electronic structure and properties of Bi [15,71,82–93]. Bi is the most challenging metal in the group five semimetals and the delicate balance between a metal and semiconductor characteristics depends crucially on the surface structure. In the case of Bi the closed-packed (111) surface can provide a metallic state. Many unique properties of this metal are related to the electronic structure and the surface geometry [94]. The bulk bismuth has a rhombohedral symmetry. Due to the atomic interaction cleaving takes place along the (111) plane. Alternately, the Bi structure can be described as hexagonal (six atoms per unit cell) or as a pseudo-cubic structure. Angle-resolved photo-emission spectroscopy (ARPES) studies have been performed for the characterization of Bi(111) surfaces indicating that the surface is a much better metal than the bulk [16,80,93,94].

Besides the low toxicity, bismuth provides similar electrochemical behavior as the toxic mercury. It has easily renewable surface, wide potential region of ideal polarizability and benefits of using solid electrode makes it desirable electrode material for anodic stripping analysis of heavy and other metal cations and electrochemical detection of organic compounds [16,80,95,96].

The Bi(111) interface is similar to graphite (0001) surface. Bismuth, as well as graphite, are chemically fairly inert in a wide range of potentials. There is practically no adsorption of O_2 and H_2O at low pressures and moderate temperatures on bismuth and this reminiscent the behavior of the graphite (0001) basal plane. These similarities make it possible to do systematic and fundamental studies in different electrolytes which can be used future for carbon materials based devices [94].

The adsorption of surface active spices and the structure of the adsorption layer are influenced by the chemical nature of the ions, electrode material, electrode potential and also by surface geometric structure [35,96–98]. The attention that bismuth surface has attached over decades is caused by the difference in the properties compared with the bulk state. The Bi(111), (110) and Bi(100) are showing much better characteristic properties for metals than the bulk due to the presence of metallic surface states. This property has a huge influence on Bi thin film and cluster investigation and in the use of Bi nanomaterials in electrochemistry or nano-electronics [80,91].

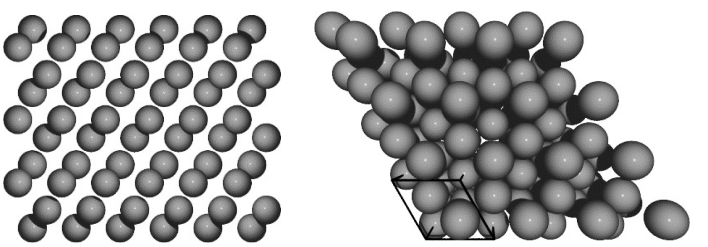

Figure 2. Calculated crystallographic structure of bismuth (111) single crystal.

4.4. Pyrolytic graphite

Carbon is a commonly used electrode material in electrochemistry due to the high chemical stability, low cost, wide variety of physical forms and opportunities for chemical modifications. Graphite, glassy carbon, carbon fibers, nanotubes, diamonds and amorphous carbon powders can be used. Pyrolytic graphite (PG) used in this work is a polycrystalline carbon electrode. PG is chemically and electrochemically stable in a wide range of potentials and in various electrolytes. The chemical reactions and corrosion starts at the crystallite edges and as PG has less defects than commercial graphite, this makes it stable electrode material. Highly oriented pyrolytic graphite (HOPG) is a special type of carbon electrodes which is comparable with single crystal metals [99–101].

PG was chosen as an electrode material because it is more similar to carbon electrodes used in SCs. HOPG is a standard substrate and is used for education purposes for AFM and STM measurements, but for the experimental point of view, the use of PG is more solid choice due to the reproducibility compared with HOPG interface as working electrode in used measurement setup [102–104].

4.5. An overview of the techniques used for electrochemical analysis in ionic liquids

The main techniques used for the electrochemical characterization of metal|IL interface are cyclic voltammetry (CV) and electrochemical impedance spectroscopy (EIS). Nowadays the detailed analysis of the surface structure of solid materials and adsorbed layers become more and more essential for the design of better (high power density) electrochemical devices. The application of scanning probe microscopies such as scanning tunneling microscopy (STM) and atomic force microscopy (AFM) in the field of characterization of ionic liquids becomes more common in every year. STM is an extremely powerful method for the atomic resolution surface analysis. Benefiting from the long-range tip-sample interactions, AFM also allows to investigate the diffuse layer region of the electrical double layer in ILs. Also molecular simulation and theoretical models are used for predicting and analyzing the interfacial structure of ILs at electrodes [28,38,105–110].

4.5.1. Cyclic voltammetry

Cyclic voltammetry (CV) is the most widely used technique for obtaining qualitative information about electrochemical characteristics of electrode|ionic liquid interfaces and the electrochemical behavior of redox active compounds in ionic liquids. Cyclic voltammetry gives information on the redox behavior of electrochemically active species, on the kinetics of electrode reactions, and in

many cases enables to observe the formation of reactive intermediates and subsequent reaction products. CV also give quantitative indication of more complex electrode processes incorporating adsorption step, being a valuable diagnostic tool in the development of analytical procedures [111,112].
A cyclic voltammogram is obtained by measuring the current at the working electrode during the potential scan. The potential of the working electrode is controlled versus a reference electrode. The current can be considered as a response to the potential excitation. The voltammogram is a display of current versus potential graph. Horizontal axis can be thought as a time axis because the potential varies linearly in time.

The characteristic peaks in the cyclic voltammograms are caused by the faradic reactions and formation of the diffusion layer near the electrode surface. A redox couple in which both pieces rapidly exchange electrons with the working electrode is termed as an electrochemically reversible couple. The peak current for a reversible couple (at 25 °C) is given by the Randles-Sevcik equation:

$$i_p = (2.69 \times 10^5) n^{3/2} A D C_c^{1/2} v^{1/2}, \quad (1)$$

where n is the number of electrons transferred, A is the electrode area (in cm^2), C_c is the concentration (in mol cm^{-3}), D is the diffusion coefficient (in cm^2s^{-1}), and v is the scan rate (in Vs^{-1}). However, the ratio of peak currents can be significantly influenced by chemical coupled to the electron process. In the case of irreversible and quasi-reversible processes, the individual peaks are reduced in size and are widely separated in potential scale. Electrochemical irreversibility is caused by slow electron exchange of the redox species with the working electrode.

Cyclic voltammetry can be used for evaluation of the interfacial adsorption behavior of the electroactive compounds. Both the reactant and product can be involved in an adsorption – desorption process. Such behavior occurs for many organic compounds, as well as for metal complexes. Usually gradual increase of the cathodic and anodic peak currents is observed, indicating progressive adsorptive accumulation at the surface.

In the case of adsorption (capacitive) behavior symmetrical cyclic voltammetry peaks are present in CV curve. Usually they are easily distinguished from ordinary diffusion-controlled peaks and a peak half-width is 90.6/n mV. The peak current is directly proportional to the surface excess (Γ) and potential scan rate:

$$i_p = \frac{n^2 F^2 \Gamma A v}{4RT}, \quad (2)$$

where, i_p is the peak current, F is the Faraday constant, Γ is the surface excess, A is the area of an electrode, v is the potential scan rate, T is the temperature and R is the gas constant. In practice, the ideal behavior is approached for

relatively slow scan rates. The situation can be more complicated when one species adsorbs on the electrode surface and adsorption peaks can be seen along with the normal diffusion controlled peaks (post-peak or pre-peak). The presence of adsorption pre-peaks is characteristic for CO-stripping voltammogramms at Pt(hkl) and Pt(poly) electrodes with higher-coverage CO addlayers [112–116].

4.5.2. Range of the measured potentials – electrochemically stable potential region

A stable supporting electrolyte and good solubility of a analyte in an electrolyte are essential for studying electrochemical processes or using electrolytes and their mixtures for various electrochemical applications. The absolute value of the potential range, were the device or electrochemical system is studied, is called with different names in the literature – electrochemical window, electrochemical stability region, voltage window, etc. Typically, the electrochemical potential window lies at a potential range in which the electrolyte is not oxidized or reduced. The electrochemical potential window is a measure of the electrochemical stability of an electrolyte against oxidation and reduction processes at selected electrode. The electrochemical potential window governs the range of the potentials available for studying the electrochemical processes that will not be affected by the electrolyte(s) and/or the solvent decomposition. For the ideally polarizable electrode, no charge transfer occurs through the interface and the current (charge) contributes merely to the establishment of the electrical double layer. The ideal polarizability region is characterized by a horizontal region of a potentiostatic *I-E* curve (so called "potential window"). Compared with different reference electrodes in the same IL system, the width of potential window should be consistent. The change of reference electrodes only affects the absolute value of potential in the most of IL systems. All reference electrode potentials can be calibrated by using a stable redox couple. For silver reference electrodes ferrocene/ferrocenium or cobaltocene/cobaltocenium ($Fc|Fc^+$ or $Cc|Cc^+$) redox couples can be used, if they behave as an ideal reference couple in a selected IL system [44,61,117,118].

4.5.3. Electrochemical impedance spectroscopy

Electrochemical impedance spectroscopy (EIS) is a powerful technique for investigation of the electrochemical systems and processes. It is widely used for the characterization of materials and devices such as power source devices, biological systems, corrosion studies, sensors, battery characterization and also for fundamental studies and system testing. EIS is noninvasive and can be used for studying interfacial processes where time constants might range from minutes down to microseconds. Impedance methods are based on perturbation of the electrochemical systems. The perturbation can be initiated by wide range

of parameters such as the applied potential, the applied current, the convection rate at hydrodynamic electrodes, or light intensity [119,120]. Usually the sinusoidal perturbation is applied to the electrochemical system:

$$V(t) = V_0 \sin \omega t, \tag{3}$$

where $V(t)$ is the voltage at time t, V_0 is the voltage amplitude, and ω is the radial frequency (in rad·s^{-1}). The relationship between the angular frequency and the frequency f is $\omega = 2\pi f$. The current response $I(t)$ will be a sinusoid at the same frequency but depending on the electrochemical system properties and can be shifted in phase.

$$I(t) = I_0 \sin(\omega t + \phi), \tag{4}$$

where $I(t)$ is the current at time t, I_0 is the current amplitude, and ϕ is the phase shift by which the voltage lags the current. Analogous to the Ohm's law, which defines resistance in terms of the ratio between input voltage and output current, the impedance can be defined as

$$Z = \frac{V(t)}{I(t)}. \tag{5}$$

Impedance is more general concept than either pure resistance or capacitor area, as it takes the phase differences between the input voltage and output current into account. Like resistance, impedance is the ratio between voltage and current, demonstrating the ability of circuit to resist the flow of electrical current, represented by the real part of the impedance Z', but it also reflects the ability of a circuit to store electrical energy, reflected in the imaginary part of the impedance Z''. The impedance can be defined as complex resistance encountered when current flows through a circuit composed of resistors, capacitors, and/or inductors. The impedance has a magnitude ($Z_0 = V_0/I_0$) and a phase ϕ and is thus a vector quantity. In complex notation impedance is presented as

$$Z = Z_0(\cos \phi + \mathrm{j} \sin \phi) = Z' + \mathrm{j}Z'', \tag{6}$$

where $\mathrm{j} = \sqrt{(-1)}$. If the Euler's formula is used, we can also write

$$Z = Z_0 e^{\mathrm{j}\phi}. \tag{7}$$

Impedance is usually presented in complex plane plots. Plot, where the imaginary part is presented versus the real part, is called also Nyquist plot.

If the sinusoidal voltage is applied to a pure resistor of value R, then $Z_0 = R$ and $\phi = 0$ (for all frequencies). In case of a pure capacitor, the impedance can be calculated according to the relationship

$$Z = \frac{1}{j\omega C} = -\frac{j}{\omega C} \tag{8}$$

where C is the capacitance. The magnitude of the impedance for a pure capacitor is

$$Z_0 = \frac{1}{\omega C}, \tag{9}$$

and the phase angle $\phi = -\pi/2$. The impedance of a capacitor depends on the frequency and is entirely imaginary. Resistance and capacitance can be combined in series or in parallel. For series connection, according to Kirchhoff's law, the current thought both elements is the same and the potential equals the sum of the potential across the capacitor and resistor. The total impedance can be calculated

$$Z = R - \frac{j}{\omega C}. \tag{10}$$

In case of parallel appeal, the complex plane diagram shows the shape of semicircle. The potentials across both circuit elements are equal, while the loaded current can be calculated from the sum of the currents flowing through resistor and capacitor. For the impedance, we can write [58,119,121,122]

$$Z = \left(\frac{1}{R} - \frac{\omega C}{j}\right)^{-1}. \tag{11}.$$

4.5.4. Fitting of impedance data

The number of different electrical double layer theories in aqueous solutions show that the charged interface between electrode and electrolyte is a very complicated system. Therefore, experimental, mathematical and computational models have been developed for better understanding of the EDL properties. EIS in combination with *in situ* STM and AFM microscopy methods are the most sensitive and informative methods for EDL experimental analysis. Calculating, modelling and fitting of the calculated data to the measured impedance data, the best knowledge about the processes and physiochemical parameters at electrode surface in terms of mathematical function can be obtained [119,122–124].

Most common (simple) analysis for EIS data is fitting it to an equivalent electric circuit model. The circuits are built from the appropriate combination of electrical elements (resistance, capacitance, inductance, Warburg diffusion element, constant phase element, etc.) representative of the electrochemical processes occurring at the electrode|electrolyte interface. In such circuit a resistor represents a conductive path of the material or the chemical step associated with an electrode faradic reaction. Capacitance is accosted with space charge

polarization regions and by specific adsorption of solution components onto an electrode. Real systems usually have nonlocal processes such as diffusion, charge motilities and defects on the electrode surface. The diffusive movement of ions under an ac field is described usually by the Warburg impedance. Electrical double layer capacitance can be replaced by the constant phase element (CPE) in the circle because the real system does not act like an ideal capacitor due to the different (adsorption/desorption) time constants, surface defects etc. The shape of the model's impedance is controlled by the electrical elements in the model as well as by the interconnections between them (series or parallel connection).

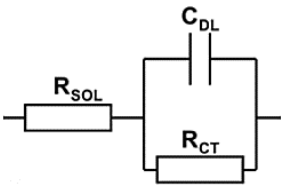

Figure 3. The Randles circuit includes an electrolyte resistance R_{sol}, charge-transfer resistance R_{ct} and a double layer capacitance C_{dl} [122].

There are lots of powerful analysis softwares, e.g., Zview, for fitting the impedance data, but still the specialized electrochemical processes (Warburg diffusion or specific adsorption) make things complicated. The most common equivalent circuit used for electrode/electrolyte system is the Randles circuit (Figure 3). This circuit describes the electron transfer processes across the electrode/electrolyte interface and the double-layer formation effect, constructed by electrolyte (solution) resistance R_{sol}, charge transfer resistance R_{ct} and a double-layer capacitance C_{dl} [66,119,122–125].

4.6. Electrode|electrolyte interface – double layer capacitance and beyond

The most prominent interest in ILs as solvents in electrochemistry comes from their good stability in wide range of electrode and cell potentials. This feature provides possibilities to investigate the electrode processes that take place at potentials beyond water electrolysis. The unique lattice saturation and adsorption of ions at electrode|IL interface make the interfacial structure much more complicated than in aqueous solutions. However, the differential capacitance is a quite well suited parameter for comparing different theories of EDL in ILs, molten salts and aqueous media. Understanding of these issues are indispensable for adequate applications of ILs in various devices. Koch and co-workers measured the differential capacitance curves of dropping mercury electrodes in $EMIm^+$ based ILs back in 1997 [126]. They believed that the classical Gouy-Chapman-Stern (GCS) model for aqueous solutions can no

longer be valid in the concentrated all-ion system. However, full and clear understanding of the interfaces requires not only the EIS data, but also atomic-resolution and molecular-level information [110,127].

Classical EDL model, suggested by Helmholtz in 1853, describes EDL mathematically as a simple plane dielectric capacitor. The term double layer can be confusing, because EDL is normally not one layer thick because of the heat motion and entropy. Thermal disorder does not allow the counter-ions to gather as a monolayer thick plane. Instead of monolayer at the polarized interfaces a space charge of ions is formed. A half century later, the Gouy-Chapman theory (GCh theory) was proposed to describe the diffuse layer formation. GCh theory offers also an easy method for estimating the value of potential of zero charge (pzc) (at least in dilute electrolytes, where the diffuse layer capacitance dominates the total one in a wide range of electrode potentials). For large electrode polarizations the compact (so-called Helmholtz) layer determines the capacitance. Important extensions for GCh theory have been made by Stern, Graham and Parson for less dilute electrolytes and in presence of specifically adsorbed ions [36,128].

Kornyshev, Fedorov and Koper [9,36,37,129,130] have proposed some theoretical models for complex metal|IL interfaces. The theoretical bell-shaped, camel-shaped and parabolic capacitance curves have been demonstrated by the experimental data at different electrodes (Hg, Au, Pt, GC, HOPG). Although the significant progress has achieved in the theoretical calculation and computational simulations of complex interfaces, the models proposed so far have not yet considered successfully the influence of the chemical nature of ionic liquids and their possible strong interactions (specific adsorption) with the surface [110,131–134]. The specific adsorption contributes to the electrode charge: ions are specifically adsorbed when short range forces dominate their interactions with the solid and these forces induce partial (or even true faradic) charge transfer between the ions and the solid. The specific adsorption may modify the shape of the differential capacitance curve and the position (in potential scale) of local capacitance minimum [110,127]. Studying the dynamics at an electrochemical interface is challenge for the computational simulations too. In principle computational calculations should provide better knowledge about factors that control the electrode kinetics, adsorption kinetics of ions, electrical potential profile, etc. There is number of attempts to characterize the electrochemical interface between ionic liquid and metal (or non-metal) electrode by computational methods combined with *in situ* STM and AFM data [38,132,135–142]. A lot of progress is done over time for *in situ* STM and AFM studies as well as for electrochemical quartz crystal microbalance (EQCM) measurements in electrochemistry. Confirming and revealing that ILs have a complex structure multilayer arrangement in the bulk phase and at the metal electrode surfaces. Like the EIS and CV, the *in situ* STM and AFM measurements show that the applied electrode potential has a strong effect on the interfacial nanostructure. At more positive or negative electrode potentials than pzc, the number of layers observed at electrode surface by AFM increases due to the enrichment of cations or anions [70,143–147].

5. EXPERIMENTAL

Electrochemical measurements were carried out in a three electrode glass cell. Before each measurement the cell and additional glassware were cleaned with H_2SO_4 + H_2O_2 mixture what was heated up to 80 °C and after that washed several times with MilliQ$^+$ water. Bi(111) single crystal and/or pyrolytic graphite (PG) were used as the working electrodes (WE). Before each measurement the Bi(111) WE was electrochemically polished in HCl + KI aqueous solution at current density about 1.5 Am^{-2}. The surface of PG electrode was prepared by the mechanical splitting of PG inside a glove box. Large surface area Pt net was used as a counter electrode (CE). CE cleaning process depends noticeably on the IL used. Basic cleaning procedure for CE was to be treated in H_2SO_4 +H_2O_2 mixture and MilliQ$^+$, but ethanol or flame treatment before the basic cleaning was needed for some electrolytes. For non-aqueous systems Ag|Ag$^+$ is the most widely used reference electrode (RE)[118]. Silver wire in glass capillary was used for prepearing a reference electrode, i.e. Ag|AgCl (or Ag|AgBr, Ag|AgI). The RE was coated with AgCl before each measurement in 0.1M HCl aqueous solution and dried 12 h at room temperature. Ag|AgCl was connected to the cell by Luggin capillary. In case of Ag|AgBr the dried electrode was treated in a mixture of $EMImBF_4$ + 5% EMImBr to exchange the Cl$^-$ for Br−. Exploring new RTILs and their mixtures containing halide ions, the stability and kinetics of the Ag|AgHal reference electrodes stability were tested. In the case of Ag|AgCl reference electrode in an iodide ion containing RTIL solution, the extremely low solubility of silver iodide, compared to that of silver chloride, causes the exchange of halide ions between a solution and the reference electrode surface. Thus, a true Ag|AgI reference electrode was formed. The rate of this process can vary widely, but in the case of I$^-$ concentration over 10 mM the exchange was fast (under 1 hour). Before the measurements WE was polarized under potential near the pzc. Before and during the polarization the additional saturation of RTIL with Ar (99.9999) was carried out. Electrochemically stable current values were established for Bi(111) and PG systems, demonstrating the stable surface conditions. Autolab PGSTAT 320 with FRA was used for cyclic voltammetry (potential cycling at different scan rates) and electrochemical impedance measurements ($0.1 < f < 10000$ Hz) inside glove box (Labmaster sp, LMBraun, O_2 and H_2O concentration <0.1 ppm).

For the *in situ* scanning tunneling microscopy (STM) measurements the Molecular Imaging PicoSTM system with Apiezon coated STM tips was used. Gwyddion and Nanotec Electronica WSXM freeware were used for the analysis of the STM data. A home-made three electrode electrochemical cell was used for *in situ* STM measurements. Similarly, to the CV and EIS measurements, Pt net was used as CE and Ag|AgCl as a RE [17,39].

1-Ethyl-3-methylimidazolium tetrafluoroborate ($EMImBF_4$) (Fluka Analytical, for electrochemistry, ≥ 99.0%, H_2O < 200 ppm, electrochemical window for GC from −2.2 V to 3.5 V, melting point 15 °C), and 1-ethyl-3-methylimidazolium

iodide (EMImI) (Merck KGaA, > 99.5%, H_2O < 300 ppm, melting point 79 °C), 1-ethyl-3-methylimidazolium trifluoromethanesulfonate (EMImOTF) (Merc KGaA, > 99.0%, melting point −12 °C) and 1-ethyl-3-methylimidazolium bromide (EMImBr) (Iolitec, ≥ 99%, melting point 73 °C) were used for preparation of the ionic liquid mixtures under study. Certain mass percentage of $EMIm^+$ with different anions were dissolved in $EMImBF_4$ at T = 80 °C (using Heidolph MR Hei-End magnetic stirrer with heating function) and cooled slowly down to room temperature (22 °C) inside a glove box (H_2O < 1.0 ppm). For the three component mixture, equal volume of $EMImBF_4$ and EMImOTF were mixed together and thereafter certain amount of EMImI was added into the mixture. Condition of heating, stirring and cooling were the same as for preparation of two component mixtures.

6. RESULTS AND DISCUSSION

6.1. Adsorption of iodide ions at Bi(111) single crystal and PG electrodes (Papers I –III)

6.1.1. Specific adsorption of iodide ions at Bi(111) single crystal electrode form ionic liquids and their mixtures (Paper I)

Previously the adsorption of iodide ions, using electrochemically polished Bi(hkl) electrodes, have been studied in aqueous electrolyte solutions and classical organic solvents [71,96,148–152]. The behavior of Bi(111) single crystal electrode in $EMImBF_4$, EMImTCB and EMImFAP ionic liquids have been characterized by Siinor et al. [153–155]. Therefore, the electrochemical characterization of the interface between Bi(111) and $EMImBF_4$ + EMImI mixture with variable concentrations were investigated by using cyclic voltammetry and electrochemical impedance spectroscopy methods. Detailed analysis of current density (j) vs. electrode potential (E) dependencies (Figure 4) shows that the Bi(111) electrode is nearly ideally polarizable within the potential region from −1.1 to −0.1 V in pure $EMImBF_4$, −1.0 to −0.2 V in 0.2% and 1% $EMImBF_4$ + EMImI mixtures and within −0.8 to −0.2 V (vs. Ag|AgCl) in 5% mixture. The increase in the current density at edge potentials is caused by the beginning of the faradic charge transfer processes. The faradic reactions at $E > -0.4$ V are caused by the oxidation of I^- ($3\ I^- - 2e \rightarrow I_3^-$) and at more positive potential ($E > -0.2$ V) also by the oxidation of the Bi electrode surface, being the main reason for the narrower ideal polarizability region compared to carbon electrodes. At more negative electrode potentials ($E < -0.8$ V) the increase in j is caused by the beginning of the reduction of residual H_2O, decomposition of BF_4^- in the presence of I^- and reduction of I_3^- to I^- ($I_3^- + 2e \rightarrow 3\ I^-$). The addition of residual H_2O in manufacturer certificate is in a good agreement with the increase in the j values at more negative potentials. EMImI (and EMImBr) contain more H_2O than $EMImBF_4$ and if the addition of EMImI (or EMImBr) increases, the current density increases.

The ideal polarizability region influences directly the energy and power density outputs of supercapacitors (SCs) as well as the presence of redox active species in the electrolyte system. In the case of redox- and pseudocapacitors, the good outcome in the presence of iodide have been shown by Frackowiak et al. [1,2,54,156].

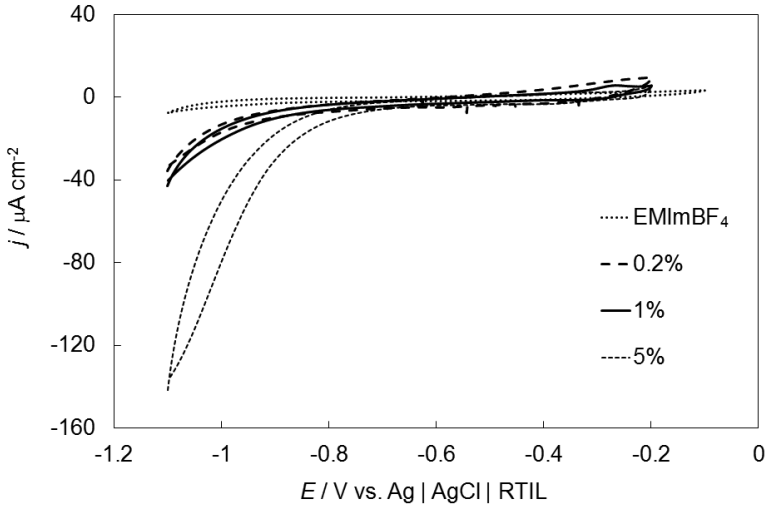

Figure 4. Cyclic voltammograms for pure $EMImBF_4$ and 0.2%, 1% and 5% of EMImI in $EMImBF_4$ at potential scan rate 10 mV/s.

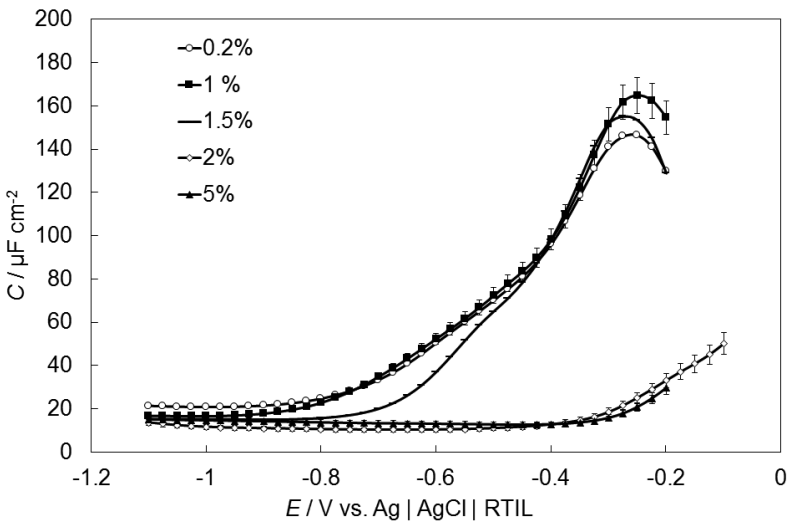

Figure 5. Experimental differential capacitance (C) vs. potential (E) curves measured at fixed ac f = 10 Hz for different EMImI concentrations in $EMImBF_4$ (noted in figure).

Influence of the I^- addition in the mixture $EMImBF_4$ + EMImI is clearly visible in the capacitance curve. The capacitance increases at less negative potentials. The analysis of the C,E curves (Figure 5) shows that the highest capacitance values for Bi(111)| I^- interface have been observed within the concentrations from 0.2% to 1.5%. For more concentrated solutions (2% and 5%) the capacitance is much lower, which could be explained by the strong adsorption followed by faradic or partial charge transfer processes between I^- ions. Thus,

bismuth surface and by the possible blocking effect of the electrode surface by the strong adsorption of I^- ions.

The same effect has been observed previously in several studies at Bi single crystal planes from aqueous and non-aqueous electrolytes in the presence of specifically adsorbed halide anions [157,158]. Compared with pure $EMImBF_4$ [157], the capacitance is higher at less negative potentials. Thus, the capacitance rises due to the presence of I^- ions in the mixture.

On the basis of practical implementation of the electrolyte for the SC (supercapacitor) the reversibility and the stability of interfacial processes are the key factors, determining the lifetime of the electrochemical energy storage system. The fastest and simplest reversibility and stability test is to measure *C*,*E* curves at fixed ac *f* first towards positive and thereafter towards negative potential directions. Smaller difference between these curves refers to better reversibility and stability of the system. According to the *C*,*E* curves (Figure 6) measured in $EMImBF_4$+ x% EMImI systems there is no remarkable hysteresis between the curves measured at f = 210 Hz. Thus, the adsorption of I^- from RTIL mixture at Bi(111) electrode is relatively reversible process.

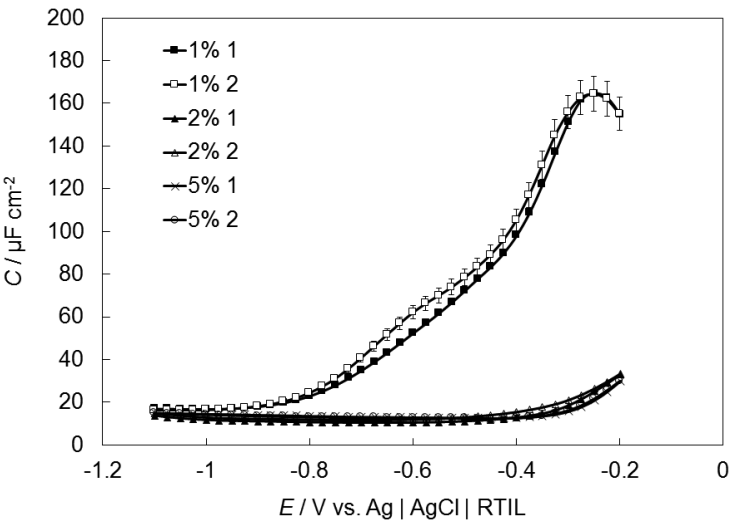

Figure 6. Experimental differential capacitance (*C*) vs. potential (*E*) curves measured at fixed as f = 210 Hz for different RTIL mixtures noted in figure first (1) towards positive and thereafter negative (2) scan directions.

Tooming et al. [159] tested the $EMImBF_4$ + 5% EMImI mixture as an electrolyte in EDLC using CV and EIS methods. The carbon material, used for electrodes, was prepared from D-glycose derived activated carbon powder, prepared by hydrothermal carbonization method followed by additional pyrolysis and carbon dioxide action steps. Noticeable increase in specific capacitance (up to 245 Fg^{-1} at 1.0 V), specific energy (36.7 $Wh\,kg^{-1}$) and specific power for EMImI + $EMImBF_4$ electrolytes have been reported. Only a minor increase in

characteristic relaxation time constant (from 1.45 s to 1.48 s) values has been demonstrated for SCs using RTIL mixture compared with pure $EMImBF_4$ [159].

Analysis of the electrochemical impedance spectroscopy data can help to understand the adsorption behavior and kinetics in a wide range of potentials and frequencies. Thereafter, non-linear fitting analysis of the impedance data can provide even better understanding of interfacial processes. The shape of complex impedance plane plots, i.e, Nyquist plots depends noticeably on the electrode potential applied (Figure 7). In the presence of specifically adsorbed ions or faradic processes outside and near the ideal polarizability region limits the dependence of the shape of the Nyquist plots enables to understand the influence of the electrode potential and frequency applied. The evaluation of the different kinetic processes that take place at the electrode surface is also possible. The phase angle and the ratio of C_p/C_s vs. frequency plots can be used as well for the electrochemical characterization.

For pure $EMImBF_4$, the shape of Nyquist plots and phase angle values do not depend noticeably on the potential applied within the ideal polarizability region [154], indicating only weak deviation from the nearly ideal capacitive behavior at Bi(111) electrode. From the literature data it is known that the rise in the capacitance curve should be connected with the beginning of the strong specific adsorption of I^- at Bi(111) electrode surface. From the Figures 7 and 8 it can be seen that the kinetic-nature of the first peaks in *C*,*E* curve (Figure 6) is mainly adsorption for 1% EMImI addition mixture. For more concentrated EMImI additions in $EMImBF_4$, there is a small deviation from adsorption limiting step behavior at lower frequencies (Figure 7). For the 0.2% and 1% mixtures within the potential region from −0.6 V to −0.2 V the specific adsorption of I^- takes place. Thus, comparing the different systems at $E = -0.3$ V the role of adsorption process is clearly visible, indicating that the adsorption of I^- is the main rate limiting process. In low *f* region, the phase angle value is lower than −75° and in moderate *f* range δ is lower than −80°.

The EDL formation shifts towards higher frequencies for higher I^- concentration mixtures compared with 0.2% and 1% mixture (Figure 8). The ratio of C_p/C_s calculated from impedance data (Figure 9), characterizes only the limiting adsorption processes at very low and moderate *f* region, without any influence of resistive processes, confirming the system behavior also visible in Nyquist and phase angle plots. According to the theory, the value of ratio $C_p/C_s = 1.0$ is characteristic of an adsorption step limited processes and $C_p/C_s = 0.5$ for the diffusion limited processes. If the ratio lower than 0.5 (or near the zero), the (faradic) charge transfer processes take place [122,124]. For the $EMImBF_4$ +x% EMImI, the ratio C_p/C_s depends noticeably on *E* applied. At $-0.6 \leq E \leq -0.3$ V, there is only a weak deviation from the adsorption limited process mechanism for 0.2% and 1% mixtures in a wide *f* range (0.1 Hz < *f* < 100 Hz) as the ratio C_p/C_s is higher than 0.92 (Figure 9). For higher EMImI concentrations (2% and 5%) and in medium *f* range (*f* > 10 Hz) the ratio C_p/C_s is almost 1, but in the low *f* range (*f* < 1 Hz) the mixed kinetic processes

(adsorption and faradic charge transfer) take place because the calculated ratio $C_p/C_s \leq 0.75$.

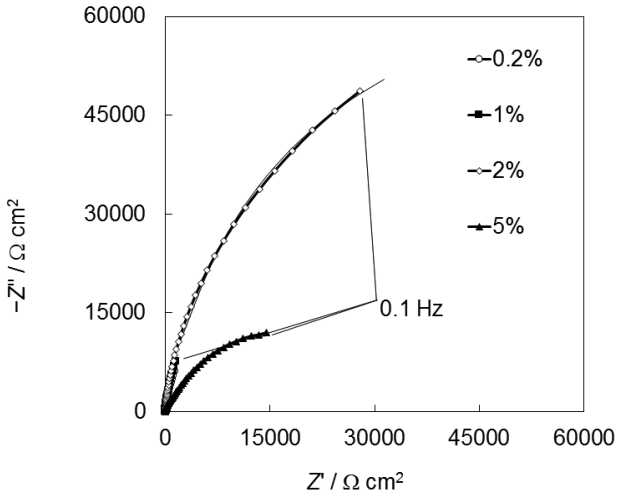

Figure 7. Complex impedance plane plots for Bi(111) electrode with different EMImI concentrations in $EMImBF_4$ (noted in figure), at electrode potential −0.3 V vs. Ag|AgCl|RTIL.

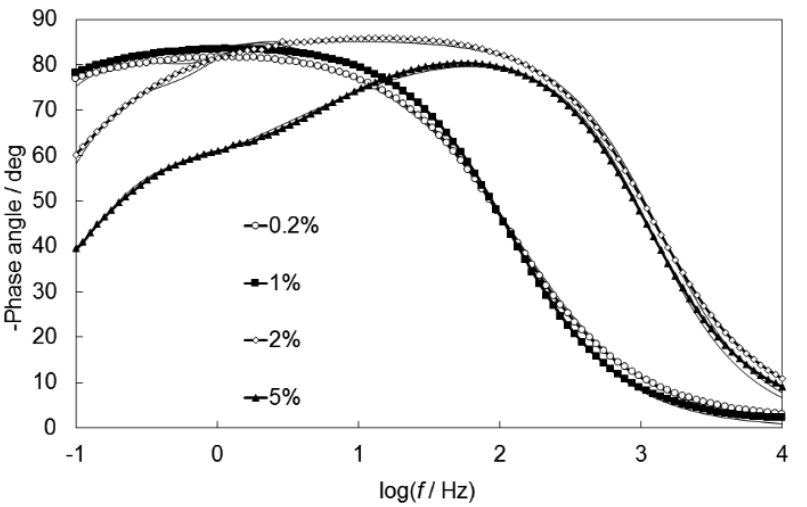

Figure 8. Phase angle vs. log f dependencies for Bi(111) electrode with different additions of EMImI in $EMImBF_4$ (noted in figure), at electrode potential −0.3 V vs. Ag|AgCl|RTIL.

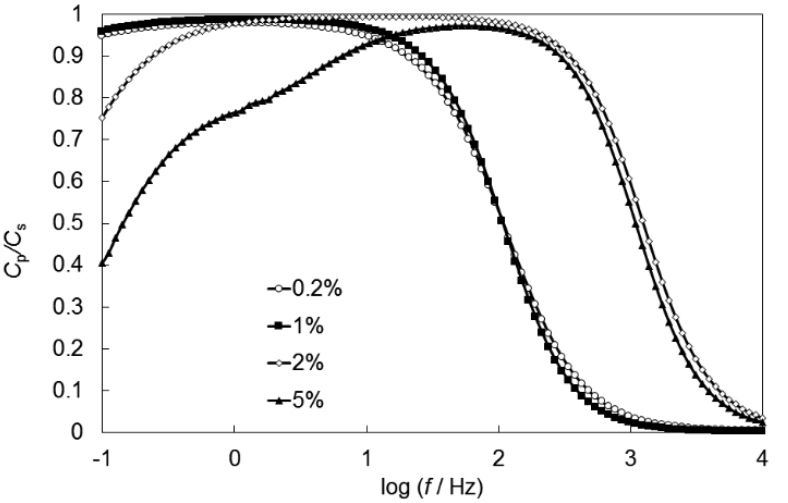

Figure 9. Calculated ratio of parallel capacitance to series capacitance vs. log *f* dependencies for Bi(111) electrode with different additions of EMImI in $EMImBF_4$ (noted in figure), at electrode potential −0.3 V vs. Ag|AgCl|RTIL.

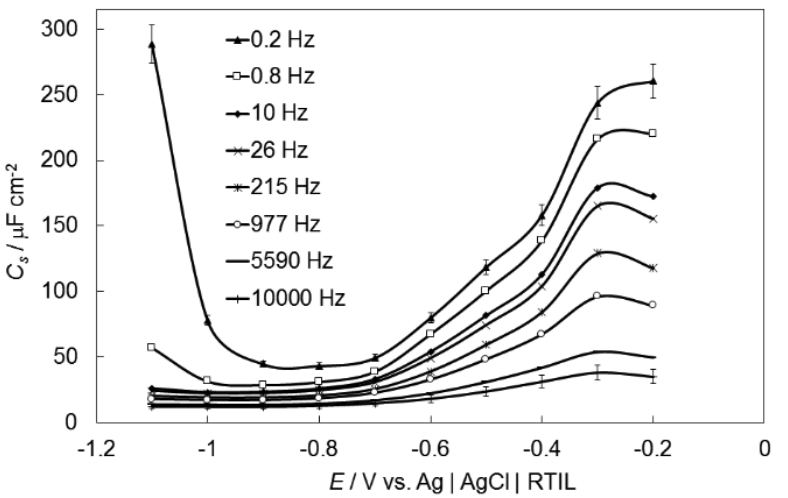

Figure 10. Series differential capacitance (C_s) vs. potential (E) curves for Bi(111) in $EMImBF_4$ + 1% EMImI at different frequencies noted in figure

It is clear that the capacitance depends noticeably on the electrode potential applied as well as on the electrode material and electrolyte composition. It is previously shown that the capacitance also depends on the frequency applied [154,155,157]. Also for studied systems (Figure 10) the capacitance values depend noticeably on the frequency and electrode potential applied. At higher frequencies the capacitance does not depend so much on the potential compared

with lower f values. This indicates to the slow nature of the interfacial processes. The rise in C_s at lower f and at less negative electrode potentials can be explained by the beginning of the specific adsorption of I^-. Moving towards more positive potentials the pseudo-capacitive behavior occurs (I^- to I_3^-). At more negative potentials (end of the ideal polarizability region), the faradic reduction processes started (I_3^- to I^-, reduction of residual H_2O etc.).

In situ STM data measured by Anderson et al. [146] for Bi(111) in $EMImBF_4$ + EMImI mixture is in a good agreement with cyclic voltammetry and impedance spectroscopy results. At the Bi(111) | $EMImBF_4$ + EMImI mixture interface within the E region from −0.7 V to −0.3 V the 2D-superstructure has been detected. The superstructure disappears at $E \geq -0.2$ V or at $E < -0.8$ V. Within the potential region of specific adsorption of I^- anions (-0.8 V $< E < -0.3$ V), the formed 2D-superstructure can be approximated to have a rhombohedral symmetry. Distances of 4.8 ± 0.2 Å have been found between the adsorbed ions centers at the Bi(111) surface. Fast Fourier transform filtering method shows an atomically flat rhombohedral surface structure at $E \leq -1.0$ V, characteristic of a clean Bi(111) electrode. Thus, the desorption of I^- takes place at high negative surface charge densities and at $E \geq -0.2$ V, quick Bi(111) dissolution (electro-oxidation) has been established [146].

6.1.2. Non-linear fitting analysis of impedance data for Bi(111)|$EMImBF_4$ + EMImI mixture

The experimental data were fitted according to the equivalent circuit shown in Figure 11. The very slow charge transfer (including partial charge transfer) processes at very low ac f have been taken into account by using the non-linear least square fitting method. The equivalent circuit used for the fitting consists of high-frequency series resistance (equal to the electrolyte resistance) R_{el}, charge transfer resistance R_{ct}, double layer capacitance C_{dl}, adsorption capacitance C_{ad} and Warburg-like diffusion impedance Z_w. The fits of calculated data to experimental data (solid lines) can be seen in Figures 7 and 8. Fitting results are rather good and the relative errors of single parameters are minor (> 10%). The high frequency series resistance R_{el} values (Figure 11) does not depend on the electrode potential applied. For $EMImBF_4$ + EMImI mixtures, the values of R_{el} are lower than those for pure $EMImBF_4$. The charge transfer resistance R_{ct} (Figure 12) depends noticeably on the concentration of I^- ions in the mixture and electrode potential applied, being higher for more concentrated EMImI mixtures. The diffusion resistance R_D values (Figure 13) for 1% EMImI mixture are lower compared with more concentrated mixtures, where R_D increases at less negative potentials. The different behavior of R_{ct} and R_D for more concentrated mixtures can be explained by the expressed repulsion effect between adsorbed I^- ions and blocking adsorption of I^- (or intermediates) at Bi(111) interface.

Similar to the previously calculated parameters, the C_{dl} and C_{ad} values depend noticeably on the concentration of EMImI in the RTIL mixture and on

the electrode potential applied. C_{dl} values (Figure 14) are lower for pure $EMImBF_4$ and for higher concentrations (2% and 5%). For mixtures with lower I^- concentrations, C_{dl} values increase similarly to the C_s values. This effect is caused by the different structure and thickness of EDL (Stern layer). The strong increase in C_{ad} values (Figure 15) indicates that the adsorption of I^- and EDL densification/optimization stages are very slow processes.

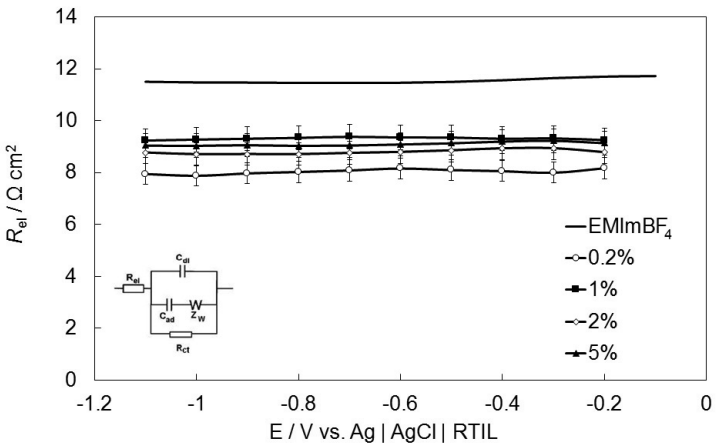

Figure 11. High frequency series resistance (R_{el}) vs. potential (E) curves for Bi(111) in different RTIL mixtures, noted in figure. Inset: equivalent circuit used for fitting the calculated data to experimental one.

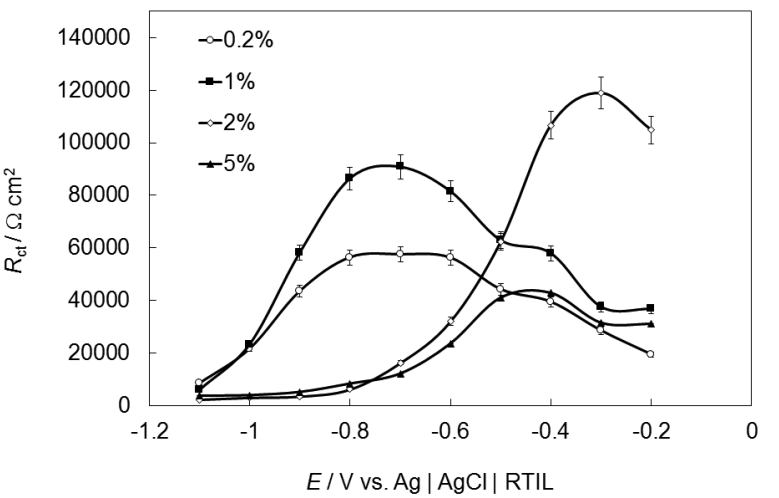

Figure 12. Charge transfer resistance (R_{ct}) vs. potential (E) curves for Bi(111) in different RTIL mixtures, noted in figure.

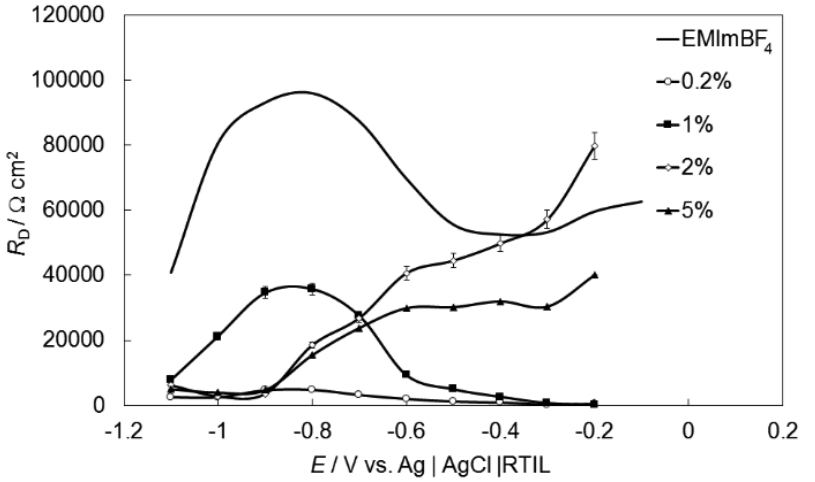

Figure 13. Diffusion resistance (R_D) vs. potential (E) curves for Bi(111) in different RTIL mixtures, noted in figure.

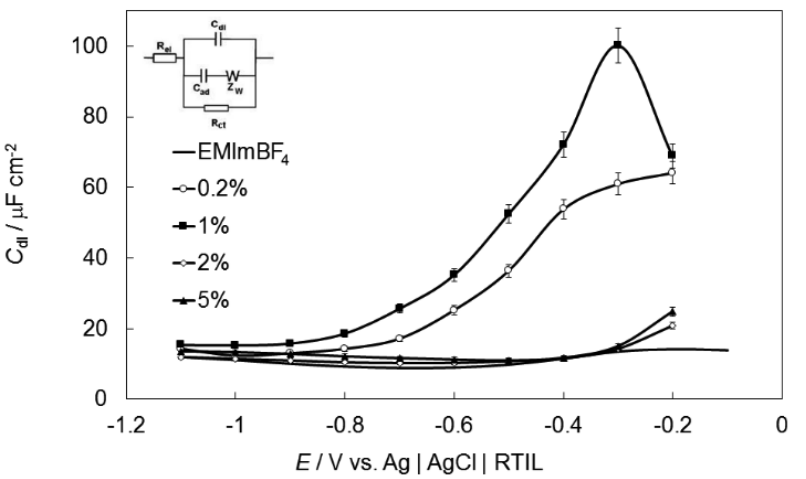

Figure 14. Dependence of double layer capacitance (C_{dl}) vs. potential (E) curves for Bi(111) in different RTIL mixtures, noted in figure.

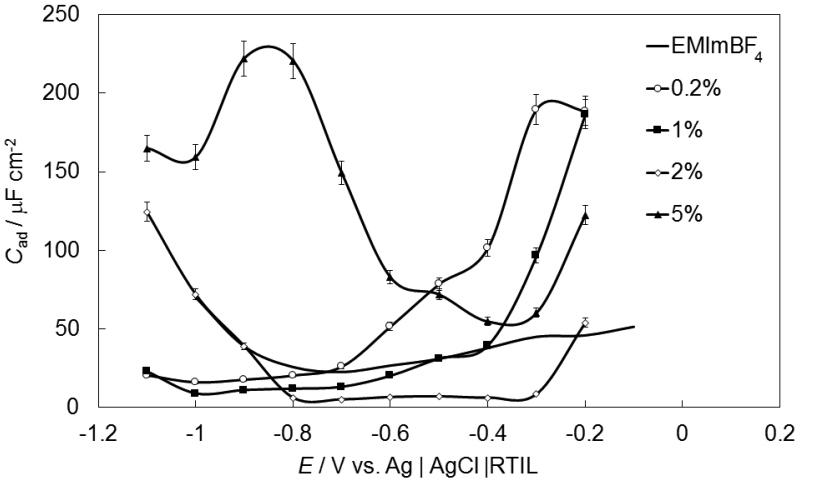

Figure 15. Dependence of adsorption capacitance (C_{ad}) vs. potential (E) curves for Bi(111) in different RTIL mixtures, noted in figure.

6.1.3. Specific adsorption of iodide ions at Bi(111) single crystal electrode form three component ionic liquid mixtures (Paper II)

For the further investigation and possible practical application of EMImI + $EMImBF_4$ mixture in modern electrochemical devices, the EMImOTF was added into $EMImBF_4$ + EMImI system (Paper I). The purpose of three IL mixture was to investigate the influence of OTF^- anion on the EDL parameters, but especially on the capacitance. The analysis of CV data (Figure 16) shows that the EMImOTF + 1% EMImI mixture is nearly ideally polarizable within −1.0 to 0.1 V. Although, for the three component mixture ΔE established was from −1.0 to −0.2 V.

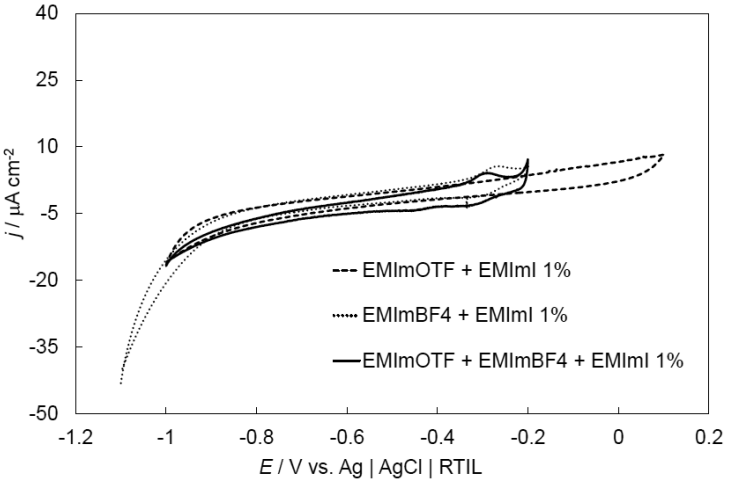

Figure 16. Cyclic voltammograms for Bi(111) electrode in different RTIL mixtures (noted in figure) at potential scan rate 10 mV/s.

For the detailed analysis of adsorption processes the EIS data were measured and analysed. From the *C*,*E* plots (Figure 17) we can see that in the case of EMImOTF + 1% EMImI the capacitance does not increase, indicating that the OFT^- hinders I^- adsorption at the Bi(111) interface. For the three component mixture, the capacitance increases at less negative potentials almost as much as in the case of $EMImBF_4$ + 1% EMImI. Only the 1% EMImI system was investigated for three component mixture, because in the case of $EMImBF_4$ + x% EMImI systems the 1% addition showed the highest capacitance values at Bi(111) interface (Figure 6). The capacitance depends noticeably on the electrode material and therefore it is not useful to optimize the electrolyte mixture (I^- concentration) at Bi(111) single crystal interface. The further investigation and testing of this highly promising three component mixture is still needed to do in SC testing system with porous carbon electrodes because the three electrolyte mixture shows comparable performance with $EMImBF_4$ + EMImI. The price of EMImOTF is cheaper than that for $EMImBF_4$. Thus, the SC with the same power and energy density can be produced with much lower price.

Surprisingly the difference between $EMImBF_4$ + 1% EMImI and $EMImBF_4$ + EMImOTF + 1% EMImI at $E = -0.3$ V in *C*,*E* curves (Figure 17) is minimal. However, there is no increase in the capacitance at less negative electrodes potentials for EMImOTF + EMImI mixture and this indicates that there is a possible blocking effect of OTF^- at Bi(111) interface. *C*,*E* curves (inset in Figure 17) measured first towards positive and thereafter negative potential scan direction for 3-component system also do not show remarkable hysteresis at $f = 210$ Hz, similarly to $EMImBF_4$ + EMImI system. Thus, in 3-component RTIL mixture, within the measured potential region $-1.0 < E < -0.2$ V, the adsorption of I^- at Bi(111) is a nearly reversible process.

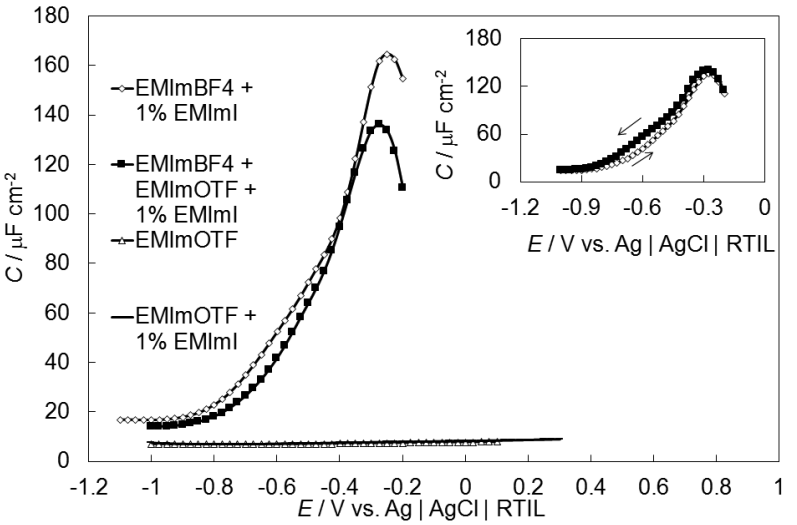

Figure 17. Experimental differential capacitance (*C*) vs. potential (*E*) curves measured at fixed ac f = 210 Hz for different RTIL mixtures noted in figure. Inset: *C*,*E* curve measured first towards positive and thereafter negative scan directions.

As for the $EMImBF_4$ + EMImI system, also for three component mixture the shape of Nyquist and phase angle plots depends noticeably on the electrode potential applied. Within the region of potentials, where the specific adsorption of I^- takes place, the nature of kinetic processes analyzed from Nyquist plots (Figure 18) is similar to the two component RTIL mixture, showing only weak deviation from adsorption limited processes at moderate and lower frequencies. For EMImOTF + EMImI systems the phase angel value differs significantly (Figure 19). The mixed kinetic processes take place at low $f \leq 10$ Hz and the phase angle, log f plots are shifted towards higher frequencies for EMImOTF + EMImI systems. If the capacitance is lower because of the blocking adsorption of OTF^-, then the adsorption of I^- is slower compared with OTF^-. So, the slow adsorption with partial charge transfer step are the rate limiting processes for I^- + OTF^- mixed anions systems.

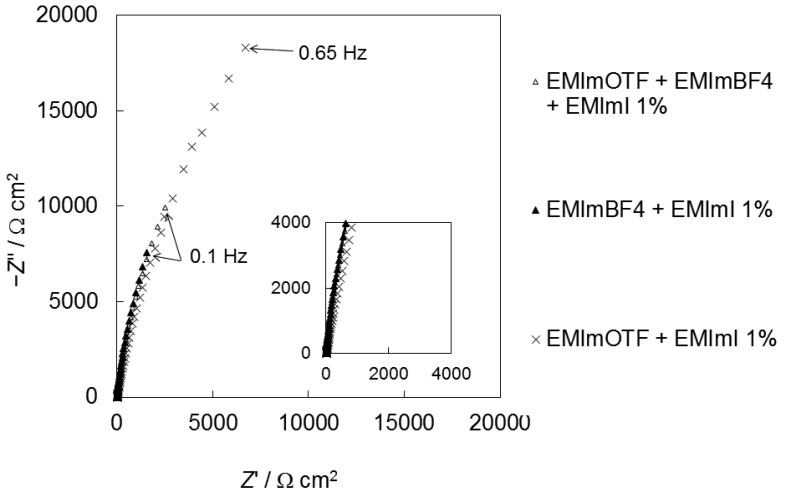

Figure 18. Nyquist plots for Bi(111) electrode in different RTIL mixtures (noted in figure), at electrode potential −0.3 V vs. Ag|AgCl|RTIL.

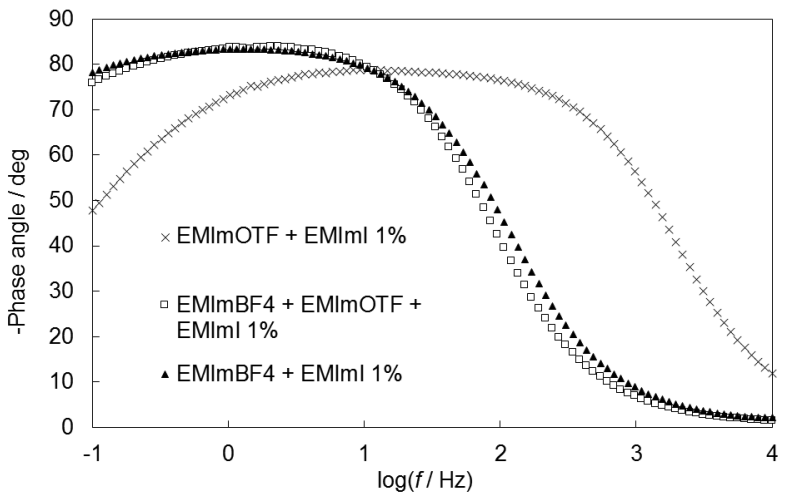

Figure 19. Phase angle vs. log *f* dependencies for Bi(111) electrode in different RTIL mixtures (noted in figure), at electrode potential −0.3 V vs. Ag|AgCl|RTIL.

Similarly, with $EMImBF_4$ + EMImI system the rise in the C_s (Figure 20) at lower *f* can be explained by the beginning of the specific adsorption of I^- at less negative electrode potentials. Moving towards positive directions the pseudo-capacitive behavior occurs (oxidation of I^- to I_3^-). At more negative end of the ideal polarizability region, the faradic reduction processes start (reduction of I_3^- to I^-, residual H_2O etc.).

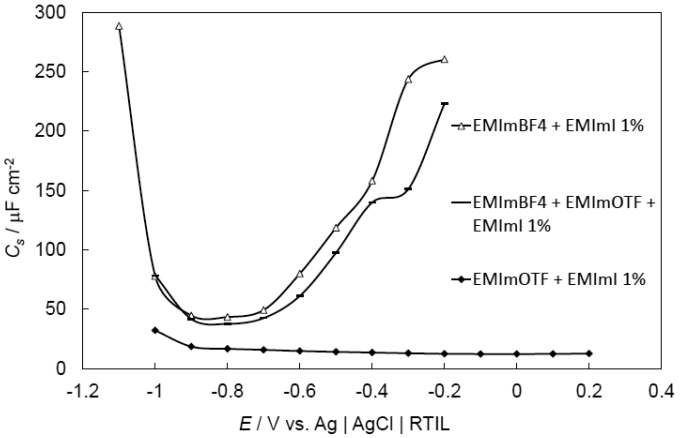

Figure 20. Series differential capacitance (C_s) vs. potential (E) curves at fixed ac $f = 0.2$ Hz for Bi(111) electrode in different RTIL mixtures noted in figure.

6.1.4. Interface between PG|EMImBF$_4$ + 5% EMImI mixture (Paper III)

Previously mentioned similarities between Bi(111) and PG can be seen also in the case of adsorption of I^- ions from EMimBF$_4$ + EMImI mixtures. The behavior of the interface between carbon electrode and aqueous electrolytes containing I^- ions have been studied previously by Frackowiak et al. [1,2] and Jänes et al. [160] in SC systems, demonstrating the positive effect of I^- additions for capacitance values as well as good long term cycle stability. The use of carbon electrode materials allows to measure in wider range of electrode potentials. For pure EMImBF$_4$ at PG interface the potential region is from −1.5 to +1.5 V without any oxidation and reduction peaks in CV curves. Based on the shape of CV curves we can say that peaks in CV for 5% EMImI containing mixtures, measured at PG interface, are caused by the addition of I^- ions (Figure 21).

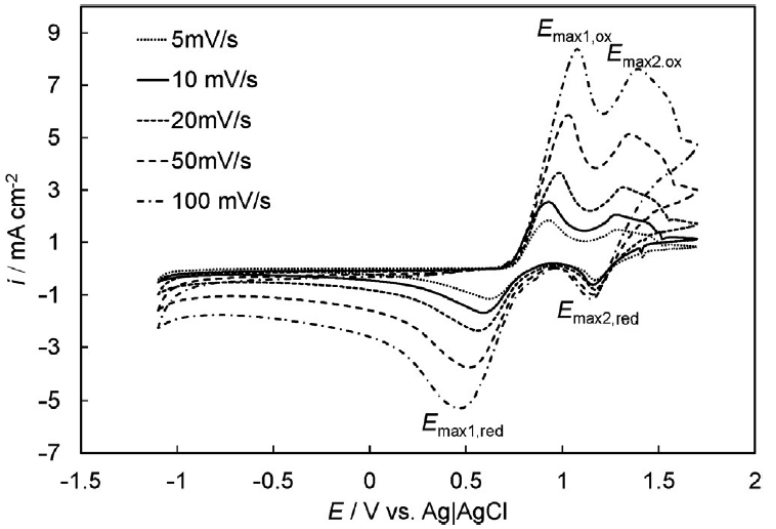

Figure 21. Cyclic voltammograms for pyrolytic graphite (PG) electrode in $EMImBF_4$ + 5% EMImI at different potential scan rates (noted in figure).

Detailed analysis demonstrates, that there are two peaks on CV curves and the difference between the peaks is higher than 58 mV. According to the theory [113] for aqueous electrolytes the difference between oxidation and reduction peaks potentials indicates to the weakly irreversible nature of the adsorption /desorption processes (quasi-reversible) at PG surface. In previously discussed Papers I and II, the good reversibility has been shown in *C*,*E* curves. Also at PG electrode the comparison of capacitance curves measured fist towards positive and thereafter negative scan directions does not show remarkable hysteresis. This indicates that the system is reversible. Also the time stability measurements showed only 10% difference between curves measured approximately within 48 h time gap and after 200 potential cycles (Figures 22 and 23).

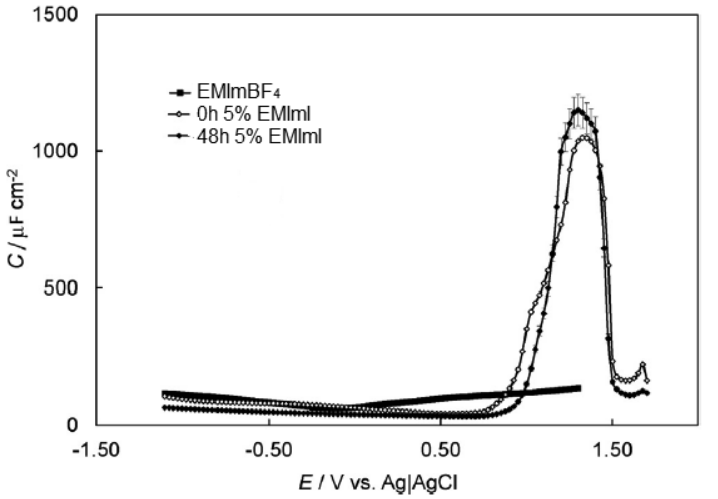

Figure 22. Differential capacitance vs. electrode potential curves for PG electrode in pure $EMImBF_4$ and 5% EMImI addition measured with 48 h time difference.

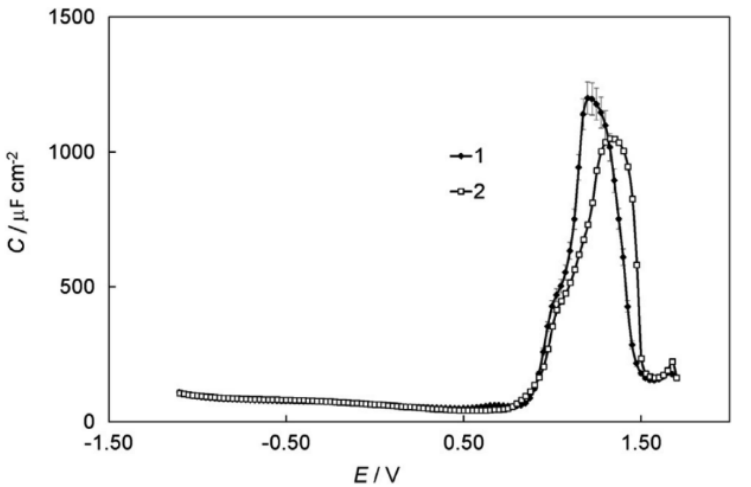

Figure 23. Differential capacitance vs. electrode potential curves for C(0001) electrode in 5% EMImI mixture measured fist towards positive and thereafter negative scan directions.

The impedance data demonstrates that similarly to Bi(111) the nature of Nyquist plots (Figure 24) or phase angle curves (Figure 25) depends noticeably on the PG electrode potential applied. The electrical double layer formation kinetics depends less on E applied at $f > 300$ Hz. The nearly ideal capacitive behavior occurs within $-0.5 < E > +0.5$ V and at lower f (100 Hz $> f >$ 0.1), were the values of phase angle are as low as −80°. Noticeable deviations from ideal adsorption behavior (and more complicated processes) are taking place at $E < -0.5$ V and $E > +1.1$ V. At the first capacitive peak region $E = +0.7$ V, the

phase angel value goes to −70° and thereafter at $f < 50$ Hz starts to increase quickly. The faradic processes are quicker than the specific adsorption processes (with partial charge transfer) and there is strong specific adsorption of I^- at PG interface. For the second peak ($+1.1 < E < +1.5$ V) the total rate of the process is limited by the faradic processes at the PG electrode. The same pseudocapacitive effect causes the rise in *C*,*E* curves in second peak region but the first peak is caused by the specific adsorption of I^-. The system shows also a remarkably good stability and reversibility in time as discussed before.

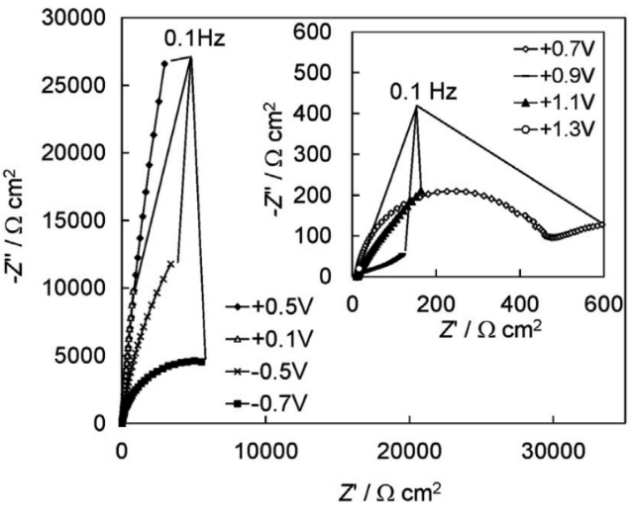

Figure 24. Nyquist plots for PG electrode in 5% EMImI + $EMImBF_4$ mixture at different electrode potentials (noted in figure).

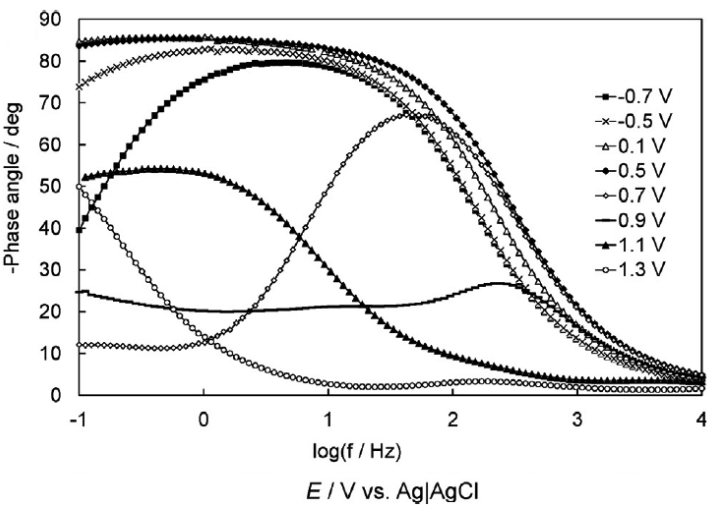

Figure 25. Phase angle vs. log frequency plot for PG in $EMImBF_4$ + 5% EMImI at different electrode potentials (noted in figure).

The nanostructure of the Stern layer between ionic liquid and graphite has been studied by Atkin et al. with AFM method [78]. Influence of the applied potential in the presence of lithium cation and chloride anion in 1-ethyl-3-methylimidazolium bis(trifluoromethylsulfonyl)imide (EMIm TFSI) on Stern layer nanostructure at highly oriented pyrolytic graphite (HOPG) interface has been analyzed. The Stern layer nanostructure changes markedly with surface potential as well as in the presence of different cations or anions even in very low concentration. There is some asymmetry at positive and negative potentials in Stern layer nanostructure reflecting the different surface affinities, packing constants and charge localization. For pure EMIm TFSI and with chloride addition the AFM shows an additional cation-rich layer on top of the ions in contact with HOPG at negative potentials. The cation to anion ratio does not permit packing into a regular structure and the observed arrangement is the best compromise between the need for the ions to pack and the requirement to neutralize the surface potential [78].

6.2. Adsorption of bromide ions at Bi(111) single crystal electrode (Paper IV)

In common to iodide, the bromide adsorption has been studied from several solvents at metal electrode surfaces [156,158,161–165]. The adsorption strength between bromide ions and Bi, Au and carbon electrodes should be slightly lower compared to iodide [156,158,161–165]. Based on this knowledge, better (and quicker) reversibility should be seen in the case of bromide ions at Bi(111). Also dynamic measurements show high thermal stability of EMImBr, up to 249 °C [165]. At the same time when first promising measurements at Bi(111) electrode interface had been conducted, Yamazaki et al. [50] reported the performance of non-aqueous EDLC based on $EMImBF_4$ + EMImBr, showing higher discharging capacitance and an excellent cyclability (98% retention after the 10000^{th} cycle). The electro-oxidation of bromide in acetonitrile and 1-butyl-3-methylimidazolium bis(trifluoromethylsulfonyl) imide has been studied by Allen et al. [166]. The direct oxidation of bromide to bromine, followed by formation of tribromide had been suggested. In RTIL media two waves were observed by using cyclic voltammetry with Pt micro-disk electrode. After the Br_2 formation the electrode kinetics was irreversible and the removal of the first electron was the rate determining step [166]. Thus, to ensure the reversibility of the system under study, the choice of potential region and current limits are crucial.

CV, EIS and density functional theory (DFT) calculations were performed in order to characterize the $EMImBF_4$ + x% EMImBr interface at Bi(111). First, the electrochemical stability region (ΔE) was analyzed for various EMImBr concentrations (Figure 26). The $\Delta E \approx 0.7$ V ($|j| < 10\ \mu Acm^{-2}$) has been established and being independent of Br^- concentration. This is also the potential region where the EIS should be carried out to ensure the reversibility of the system.

The increase in j (at less negative potentials) is usually caused by the oxidation or adsorption of the analyte components. In the case of Bi(111) also the electro-oxidation of electrode surface can take place at less negative potentials. Figures 26 b and c were measured in decreasing potential scan rate directions and in wider range of potentials compared with Figure 26a. Clear oxidation and reduction peaks were measured (forfeit the Bi(111) electode at slower scan rates for 2% EMImBr RTIL mixture). Although, the ΔE is almost independent of the concentration of EMImBr, there is a shift of current peaks towards more negative potentials within the increase of EMImBr concentration in the mixture. This shift can be explained by the adsorption and oxidation of Br^- ions at less negative electrode potentials and due to the reduction of Br_3^- to Br^- at more negative potentials [166].

The rapid increase in positive current density values at less negative electrode potentials $E \geq -0.8$ V (vs. Fc/Fc^+) can be explaned by the specific adsorption of Br^- at Bi(111) electrode surface, followed by the faradic charge transfer step (in agreement with EIS data, discussed later). Two oxidation peaks and one reduction peak for 0.1% and 2% EMImBr mixture were observed (Figure 26 b and c). The linear dependance of oxidation peaks current densities indicates to the adsorption limited processes and the reduction peak current densities on the square root of potential scanning rate characterise the mass transfer limited process. However, at very slow scanning rates a small deviation from linearity can be seen. The potential of the first small oxidation peak depends weakly on the potential scan rate (Figure 26b), confirming the hypo-thesis that the adsorption step is the rate limiting stage. However, after applying the less negative electrode potentials there is linear dependence of reduction (desorption) peak potentials on the square root of potential scanning rate and the desorption is limited by the mixed kinetic processes. Even more complicated dependence of E_{peak} on $\sqrt{v}$ can be seen for 2% Br^- mixture (Figure 26c). Increasing Br^- adsorption, electro-oxidation of Bi(111) electrode surface as well as the formation of surface compounds take place. For more detailed studies in wider range of potentials the electrode form carbon material is more suitable, similarly to I^- (Paper III). Thus, all differential capacitance and impedance measurements have been carried out at more negative potentials than $E \geq -0.8$ V.

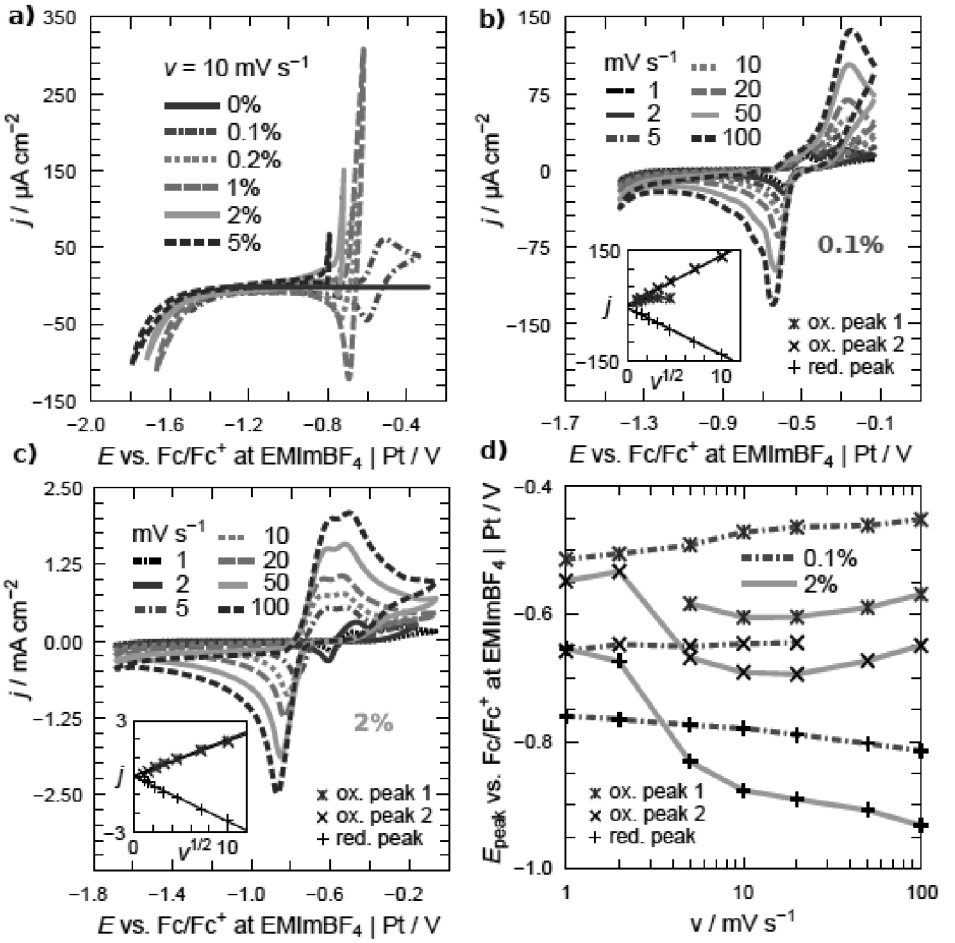

Figure 26. Cyclic voltammograms for Bi(111) electrode in different EMImBr + $EMImBF_4$ mixtures (noted in figure) at potential scan rate 10 mV/s (a), cyclic voltammograms for 0.1% EMImI mixture (b) at different potential scan rates (noted in figure), for 2% EMImI mixture (c) at different potential scan rates (noted in figure), peak potential dependence on potential scan rate for 0.1% and 2% EMImBr in $EMImBF_4$ (d).

The *C* vs. *E* curves in Figure 27 show that the capacitance increases at less negative electrode potentials for EMImBr + $EMImBF_4$ mixtures, in comparison with pure $EMImBF_4$. However, there are two different peaks in *C*,*E* curve, indicating to the existence of two different electrochemical processes. From the cyclic voltammetry data the nature of first peak showed adsorption step limited behavior and analysis of the *C*,*E* curves leads us to the same result. There is no hysteresis between curves measured first towards positive and thereafter negative potential scan directions showing that the system has good reversibility within this potential region. From the Figure 27c, it can be seen, that the

specific adsorption of bromide ions is probably followed by the faradic (partial) charge transfer. For the further investigation the electrochemical impedance data have been measured and analyzed.

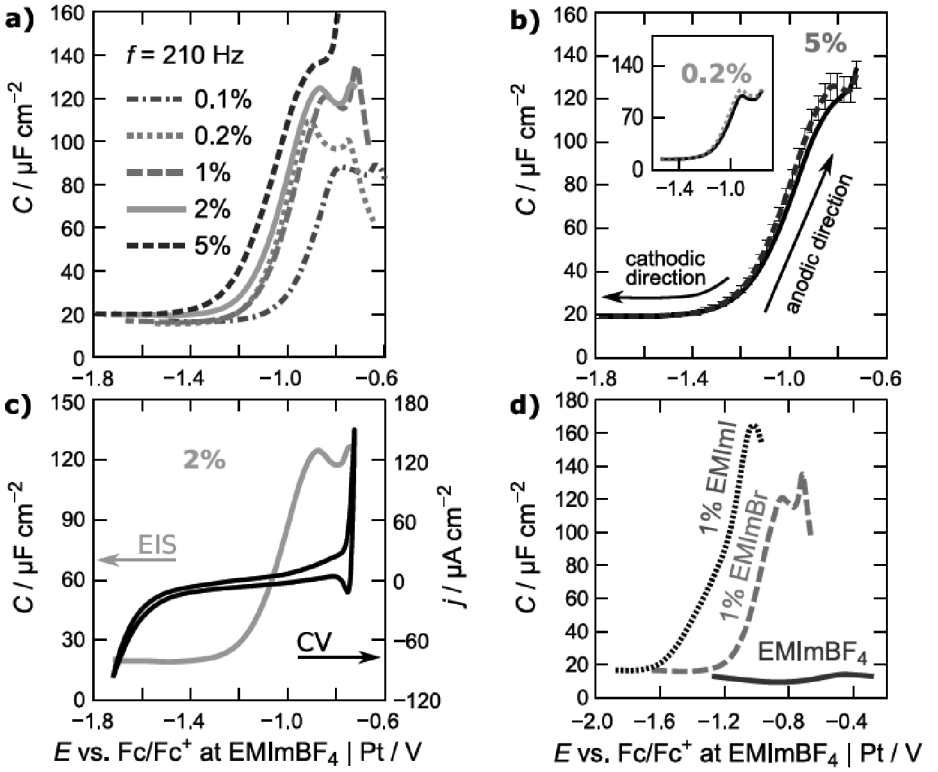

Figure 27. Experimental differential capacitance (C) vs. potential (E) curves at the fixed ac frequency (f = 210 Hz) for different EMImBr additions in $EMImBF_4$, noted in figure (a), C,E curves measured first towards positive and thereafter negative potential scan directions at the fixed ac frequency (f = 210 Hz) for 0.2% and 5% EMImBr concentrations in $EMImBF_4$ (b), comparison of C,E curve at the fixed ac frequency (f = 210 Hz) and cyclic voltammogram curve for 2% EMImBr in $EMImBF_4$ (c), comparison of different RTIL mixtures (noted in figure) at the fixed ac frequency (f = 210 Hz) (d).

Previously the halide adsorption in non-aqueous solvents at Bi(111) have been analyzed and the rise in capacitance curve at less negative electrode potential has been explained by the specific adsorption of anions, as well as by the strengthening of covalent nature of the adsorptive bond between halide ions and the electrode surface [96]. To avoid the irreversible adsorption and faradaic processes at Bi(111), the impedance measurements were carried out only within the range of the potentials from $-1.7 \leq E \leq -0.8$ vs. Fc/Fc^+ this ensures the reversibility of the system.

Nyquist and phase angle plots (Figures 28 and 29) show that the rate of the formation of electrical double layer depends significantly on the electrode potential applied. Nearly ideal capacitive behavior occurs in wide range of moderate frequencies ($0.5 \leq f \leq 100$ Hz). If the phase angle value is near −90°, then the system shows ideal capacitive behavior. At the first capacitance and current peak region the phase angle has more negative values than −82°. Thus, decrease of the phase angle values and the rise in the capacitance values in the *C*,*E*-curves (Figure 27) are mainly caused by the specific adsorption of Br^- anions onto Bi(111). At very low *f* region some deviation form adsorption limitation is probably caused by the oxidation of Br^- to Br_3^-. At the second peaks potential region the true faradic processes with charge transfer are dominating with mass transfer limitation. This conclusion has been confirmed by the phase angle value $\delta \geq -40°$ in the wide range of *f*.

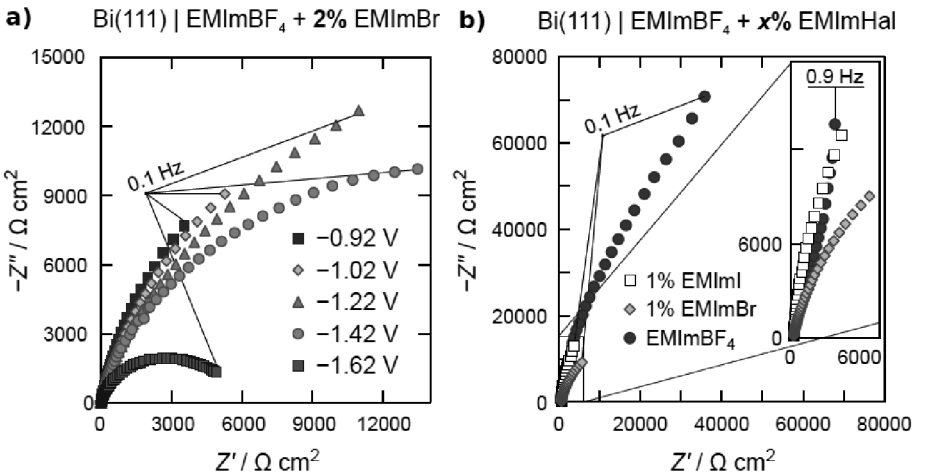

Figure 28. Complex impedance plane plots, i.e. the imaginary part (*Z*'') vs. the real part of the impedance (*Z*') dependences for Bi(111) electrode in 2% EMImBr addition in $EMImBF_4$ at different electrode potentials (noted in figure) (a). Comparison of *Z*'' vs *Z*' plots at capacitance peak potentials for different RTILs (noted in figure) (b).

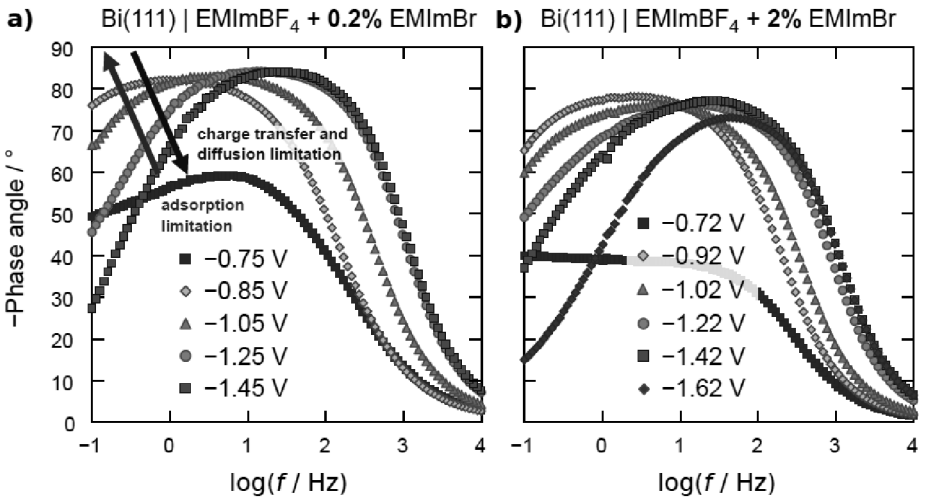

Figure 29. Phase angle vs. log frequency plots for Bi(111) electrode at RTILs interface at different electrode potentials and EMImBr concentrations in $EMImBF_4$ (noted in figure).

At more negative potentials ($E \leq -1.40$ V) the deviation from the ideal capacitive behavior can be seen. The EIS data show that various mixed kinetic processes are occour, especially at lower frequency region. Desorption of bromide species from the electrode surface, hydrogen evolution (caused by the reduction of residual H_2O [167]) and reduction of Br_3^- are taking place [50,166]. From the log $|Z''|$ vs. log f plots (Figure 30) it can be seen that within the potential region from −1.45 to −0.85 V for 0.2% mixture and from −1.42 to −0.92 V for 2%mixture (if $f \geq 0.5$ Hz), the dependences are straight lines. This is characteristic for adsorption step limited process [124]. Noticeable deviation from adsorption step limited behavior can be seen at very low frequencies and at edge potential of measured potential region. Thus, the adsorption/desorption followed by the faradic reduction of Br_3^- complex anion and residual H_2O are main limiting processes at very low frequencies at more negative electrode potentials (at $E \leq -1.45$ V).

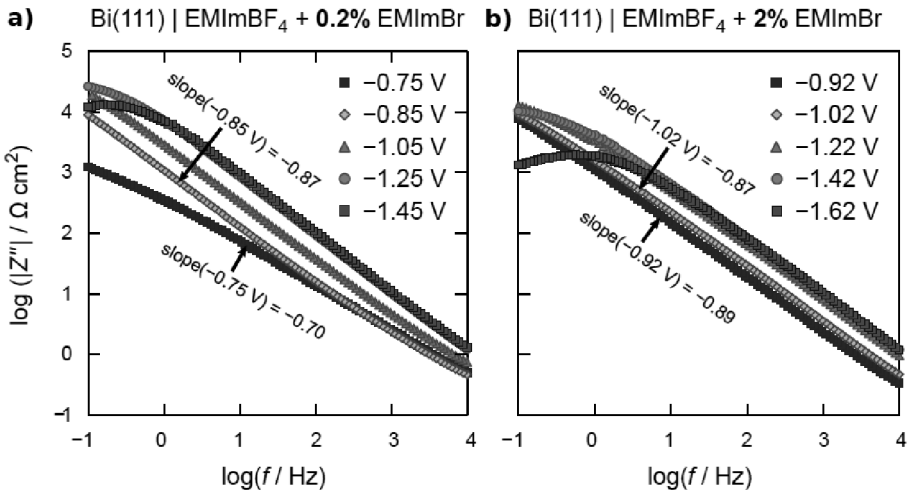

Figure 30. Log |*Z*'| vs. log *f* plots for Bi(111) electrode in different EMImBr additions in $EMImBF_4$ (noted in figure) at different electrode potentials.

The values of series capacitance and parallel capacitance (C_p) were calculated from impedance data at several fixed frequencies ($C_s = -(Z''2\pi f)^{-1}$ and $C_p = C_s/(1 + (Z'/Z'')^2)$) [124]. The C_p vs. log *f* plots in Figure 31 are in a good agreement with previously discussed cyclic voltammetry, Nyquist and Bode plots data, showing that the adsorption is the main rate limiting process at $f \leq 100$ Hz within the wide potential region applied. The increase in C_p values indicates that the there is only small influence of faradic processes at Bi(111)| RTIL mixture interface.

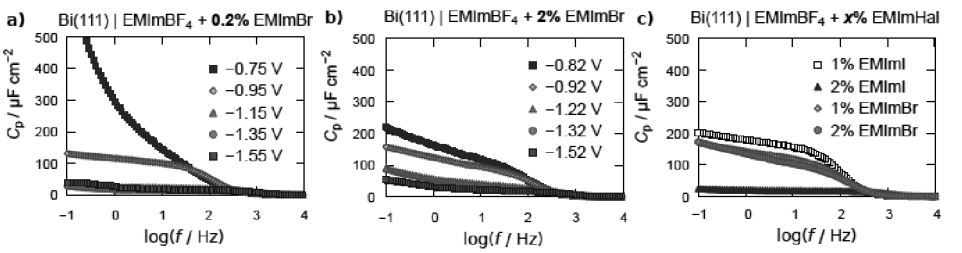

Figure 31. Parallel capacitance (C_p) vs. log frequency (*f*) dependencies for Bi(111) at different electrode potentials and EMImBr additions in $EMImBF_4$ (noted in figure) (a and b). Comparison of C_p vs. *f* curves for different RTILs (noted in figure) at capacitance peak maximum potentials (c).

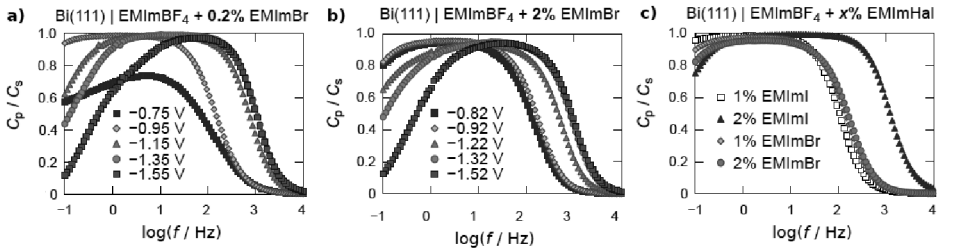

Figure 32. Calculated ratios of parallel capacitance (C_p) to series capacitance (C_s) vs. log f dependences for Bi(111) in different EMImBr concentrations in $EMImBF_4$ at different electrode potentials (noted in figure) (a and b). Comparison of C_p/C_s vs. log f dependencies at capacitance peak potentials for different RTILs (noted in figure) (c).

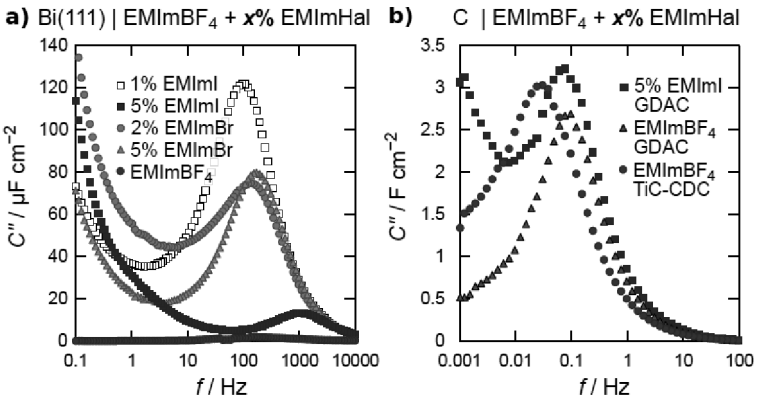

Figure 33. Calculated dependencies of imaginary part of the capacitance (C") vs. log frequency for Bi(111) electrode|RTIL interface at capacitance peak potentials (a) and for two electrode capacitor system with D-glycose derived activated carbon powder (GDAC) and TiC-CDC electrodes (b).

The C_p vs. log f plots, the ratio of C_p/C_s and the values of imaginary part of C" ($C" = Z'/(2\pi f|Z|^2)$) are widely used for the analyze of supercapacitors. Thus, the following graphs in Figures 31, 32 and 33 were composed. According to the theory, the ratio of $C_p/C_s = 1$ is characteristic for an adsorption limited processes, $C_p/C_s = 0.5$ for a diffusion limiting step. In the real systems, the ratio depends noticeably on the electrode potential applied [124,168,169].

From the Figure 31 it can be conclude that for Br^- containing system, the 2% mixture is better elextrolyte for capacitors than 1%, differently form the I^- systems, were the blocking adsorption at Bi(111) occours already for 2% EMImI system. Also the C_p/C_s vs. log f plots (Figure 32 a and b) indicate that the Bi(111)|$EMImBF_4$ + x% EMImBr system is nearly ideally polarizable within $-1.4 < E < -0.8$ V, characterizing the adsorption limited step process ($C_p/C_s = 1$, if Br^- concentration is lower than 1%). The same conclusion was valid for 1% EMImI + $EMImBF_4$ mixture. Deviation from the ideal capacitive behavior takes place at $f < 1$ Hz for both (I^- and Br^-)1% and 2% mixtures studied. The

maximum in imaginary capacitance curve (Figure 33), f_{max}, determines the characteristic time constant $\tau = (2\pi f_{max})^{-1}$ of the Bi(111)|RTIL mixture that allows to estimate the electrolyte potential limit applicable in supercapacitors.

For the Bi(111)|RTIL mixture interface, the imaginary capacitance values are noticeably lover, as expected, in comparison with the carbon materials|RTIL interface (in this case TiC-CDC is the Ti-carbide derived carbon and GDAC is the D-glycose derived carbon) (Figure 33). The charging/discharging time is shorter for Br^- containing mixtures compared with I^-, thus, the Br^- containing mixture is probably more effective electrolyte for carbon materials based supercapacitors. Also the choice of carbon material is very important (as seen in Figure 33b). For D-glycose derived carbon material the value of τ for $EMImBF_4$ + EMImI mixture is 1.48 s being slightly longer (τ = 1.45 s) than that for pure $EMImBF_4$. The calculated τ values are very short charging/discharging times for capacitors, but for TiC-CDC material the characteristic relaxation time is almost two times longer (τ = 2.80 s) [159,170]. Thus, we believe that the mixtures containing Br^- could be used for development of the higher energy-power density electrochemical energy storage devices, compared with I^- based systems.

For the detailed evaluation of electrode-anion bonding effect the DFT calculations were made. For the Bi(111) surface, the nature of the interaction of different halides does not change much, while the Au(111)–halide anion interaction type changes from ionic to covalent in the order: F^-, Cl^-, Br^-, I^-. The difference between bromide and iodide adsorption is expected to be small by DFT calculation and this is confirmed by the experimental data.

The adlayers structure of bromide at Au(hnk) interface have been studied by many authors [171–174]. Like other halides, bromide also has strong specific adsorption interactions with gold interface enabling the clear visualisation with AFM and STM methods. Definitely more investigations are needed for IL media at different electrode materials (HOPG, Bi, etc.). For conforming the data measured by electrochemical impedance spectroscopy and develop better computational methods for calculations, visualization of adsorbed ions is inevitable. Thorough, systematic investigations are necessary for developing better theories and models for EDL and furthermore, predicting the interfacial properties by computational methods.

6.3. Comparison of halide ions adsorption at Bi(111) and PG electrodes from ionic liquids media

Systematical analysis of adsorption data demonstrates that the region of ideal polarizability depends on the electrode material, on the chemical nature of specifically adsorbed anion as well as on the concentration on ions at electrode surface. Also residual water and other impurities can have crucial influence on the system characteristics under study. The ideal polarizability region for $EMImBF_4$ + 1% EMImI mixture at Bi(111) is from −1.0 to −0.2 V ($\Delta E \approx 0.8$ V) and −1.1 to −0.1 V ($\Delta E \approx 1.2$ V) for pure $EMImBF_4$. For pure $EMImBF_4$|PG

interface the region of ideal polarizability is $\Delta E \approx 3$ V (−1.5 to +1.5 V), without any current or capacitance peaks in CV or *C*,*E* curves. In the presence of 1% $EMImBF_4$ + EMImI the current peak can be seen at −0.7 V. Therefore, it is reasonable to evaluate the overall ΔE not exact potentials for different mixtures. However, using PG instead of bismuth (111) electrode allows us to measure further at more positive electrode potentials. In the presence of OTF^- anion in the three component mixture $EMImBF_4$ + EMImOTF + 1% EMImI the $\Delta E \approx 0.8$ V at Bi(111) interface. For EMImBr + $EMImBF_4$ mixtures the $\Delta E \approx 0.7$ V and does not depend noticeably on the concentration of Br^- ions in the RTIL mixture.

The shape of the *C*,*E* curve for $EMImBF_4$ + 1% EMImI, EMImOTF + $EMImBF_4$ + 1% EMImI as well as for $EMImBF_4$ + 1% EMImBr mixtures shows increase in capacitance at less negative electrode potentials. In I^- and Br^- containing RTIL mixtures the rise is significantly higher compared with that for the pure $EMImBF_4$ and EMImOTF. So we can conclude that the rise in the capacitance values is due to the presence of halide ions in the RTIL mixture. Only for the EMImOTF + 1% EMImI mixtures the capacitance does not increase in measured potential region at less negative electrode potentials. This can be explained by the possible blocking of the Bi(111) electrode surface with OTF^- anions. Although, there is not yet adequate model for describing the EDL parameters in ILs in the presence of specifically adsorbed ions. Even using simple Helmholtz model the difference in capacitance values can vary enormously, if the studied ions are different [61]. The capacitance values for the mixtures with Br^- at (210 Hz) are only slightly lower than those for I^- containing RTIL mixtures. Compared with the I^- containing RTIL mixtures, the main difference is that for Br^- containing RTIL mixtures the maximum capacitance values depend more on the EMImBr concentration within the concentration range up to 5%. Surprisingly, for more concentrated I^- mixtures the capacitance values decrease due to the strong blocking adsorption or formation of strongly adsorbed faradic reaction intermediates, which is not seen in the Br^- containing mixtures.

Analysis of the EIS data conforms that for halide ions under study the strong specific adsorption followed by the faradic (or partial) charge transfer at Bi(111) interface. It should be noted that PG and HOPG are more suitable electrode materials for studying the oxidation processes at less negative electrode potentials compared with Bi(111) due to the electro-oxidation of the Bi(111) electrode interface. All systems under study showed good reversibility and stability, if the potential region was not wider than the ideal polarizability region mentioned before. Somewhat higher reversibility and stability has been observed in case of $EMImBF_4$ + EMImBr mixtures.

Density functional theory calculations suggest that the adsorption of bromide is as strong and favourable as of iodide and could be stronger than of chloride (Paper IV). Moreover, for the Bi(111) surface, the nature of the interaction of different halides does not change much, while the Au(111)–halide anion interaction changes from ionic to covalent in the order of halides: F^-, Cl^-, Br^-, I^-. The difference between bromide and iodide adsorption is expected to be small

and this is supported by the experimental observation of the capacitance values for $EMImBF_4$ + *x*% EMImBr and $EMImBF_4$ + *x*% EMImI electrolytes. Thus, we believe that the mixtures containing Br^- could be used for development of the electrochemical energy storage devices characterized with high energy and excellent power density.

Based on the adsorption data collected for aqueous and classical organic solvents (methanol, ethanol, acetonitrile, etc.) it is known that adsorption (Gibbs) energies increase in order: $Cl^- < Br^- < I^-$ as the solvation energy of ions decreases [5,148,150,152,158]. It is surprising that in RTIL media, where the presence of solvation shell by water or other solvent is not present, within the measured concentration range the I^- ions have only slightly higher capacitance values compared with Br^-.

There are number of studies of halide ions adsorption at different electrode materials (Au, Ag, Pt, etc.) from aqueous solutions. In addition, many computational studies have been concluded. Unfortunately, there are not yet systematic studies of halides adsorption from IL media at different electrode materials. From the theoretical analysis point of view, more experimental and computational data is needed to improve the understanding of ionic adsorption of metal|RTIL interface. Results established and analysed by Koper et al. [9] show that isotherms obtained at different ionic strengths and for different solvents could give us better understanding which models should be used for correct analysis of specific adsorption data including the long range electrostatic interactions [175–178].

SUMMARY

Cyclic voltammetry and electrochemical impedance spectroscopy have been used for the electrochemical characterization of the interface between Bi(111)|RTIL mixture with the presence of specifically adsorbed I^- and Br^- anions in $EMImBF_4$ mixture. Graphite electrode (PG) has been used for the I^- anions containing mixture to investigate the system behavior at less negative electrode potentials. Also the EMImOTF was added into EMImI + $EMImBF_4$ mixture to investigate the influence of the presence competitive anion adsorption on the EDL parameters. Measurements were carried out in various range of electrode potential at Bi(111)|RTIL interface $\Delta E \approx 1.2$ V for pure $EMImBF_4$, 0.8 V for EMImI mixtures, 0.8 V for three component mixture and 0.7 V for EMImBr mixture; at PG|$EMImBF_4$ and for PG|$EMImBF_4$ + 5% EMImI mixtures the measured region was ~3 V. Thus, it was established that the region of ideal polarizability depends on the electrode material under study. The ideal polarizability region depends noticeably on the electrode material as well as on the RTIL mixture chemical composition and on the concentration of the specifically adsorbed ions in the mixture.

The difference between maximum capacitance values for I^- and Br^-, established for Bi(111), is much smaller compared with aqueous solutions indicating that the Gibbs adsorption values are comparable. Calculated DFT data show also slight differences between halide ions and the order of anions activity is in a good agreement with experimental and literature data. Good reversibility and remarkable stability of $EMImBF_4$ + EMImBr mixtures at measured potential regions have been showed. Thus, we can say the nearly physical adsorption of Br^- compared with I^- adsorption at Bi(111) takes place. The presence of competitive OTF^- anions adsorption from three component mixture did not influence the capacitance values as much as from two component mixture composed of EMImOTF + EMImI.

The model system of Bi|RTIL mixture works nicely and have been confirmed by the similar results in PG|RTIL mixture interface. Furthermore, the measured RTIL mixtures tested in SCs showed also promising results. Visualized structure of I^- ion at Bi(111) from $EMImBF_4$ by *in situ* STM allows to develop and understand the complicated interfaces between electrode|RTIL mixture and develop adequate models in the presence of specifically adsorbed ions in electrolyte mixtures.

REFERENCES

[1] G. Lota, E. Frackowiak, Electrochem. Commun. 11 (2009) 87–90.
[2] G. Lota, K. Fic, E. Frackowiak, Electrochem. Commun. 13 (2011) 38–41.
[3] J. Leddy, V. Birss, P. Vanýsek, Historical Perspectives on the Evolution of Electrochemical Tools, The Electrochemical Society, 2004.
[4] W. Schmickler, E. Santos, Interfacial Electrochemistry, Springer Science & Business Media, 2010.
[5] K. Lust, M. Väärtnõu, E. Lust, Electrochimica Acta 45 (2000) 3543–3554.
[6] D.V. Tripkovic, D. Strmcnik, D. van der Vliet, V. Stamenkovic, N.M. Markovic, Faraday Discuss. 140 (2008) 25–40.
[7] D.R. MacFarlane, K.R. Seddon, Aust. J. Chem. 60 (2007) 3–5.
[8] T. Pajkossy, D.M. Kolb, Electrochimica Acta 53 (2008) 7403–7409.
[9] M.T.M. Koper, J. Electroanal. Chem. 450 (1998) 189–201.
[10] M.T.M. Koper, R.A. van Santen, Surf. Sci. 422 (1999) 118–131.
[11] P.W. Bridgman, Proc. Am. Acad. Arts Sci. 60 (1925) 305–383.
[12] P.V. Popat, N. Hackerman, J. Phys. Chem. 62 (1958) 1198–1203.
[13] Z. Kerner, T. Pajkossy, Electrochimica Acta 47 (2002) 2055–2063.
[14] R. Costa, C.M. Pereira, F. Silva, Electrochimica Acta (n.d.).
[15] E. Lust, A. Jänes, K. Lust, R. Pullerits, J. Electroanal. Chem. 431 (1997) 183–201.
[16] T. Romann, S. Kallip, V. Sammelselg, E. Lust, Electrochem. Commun. 10 (2008) 1008–1011.
[17] S. Kallip, H. Kasuk, V. Grozovski, P. Möller, E. Lust, Electrochimica Acta 53 (2008) 4035–4045.
[18] N. Batina, A.S. Dakkouri, D.M. Kolb, J. Electroanal. Chem. 370 (1994) 87–94.
[19] K.M. Robinson, I.K. Robinson, W.E. O'Grady, Surf. Sci. 262 (1992) 387–394.
[20] A.A. Aal, R. Al-Salman, M. Al-Zoubi, N. Borissenko, F. Endres, O. Höfft, A. Prowald, S. Zein El Abedin, Electrochimica Acta 56 (2011) 10295–10305.
[21] K. Izutsu, Electrochemistry in Nonaqueous Solutions, Wiley-VCH, 2009.
[22] K. Lu, Materials in Energy Conversion, Harvesting, and Storage, John Wiley & Sons, 2014.
[23] M. Winter, R.J. Brodd, Chem. Rev. 104 (2004) 4245–4270.
[24] A. Lewandowski, A. Olejniczak, M. Galinski, I. Stepniak, J. Power Sources 195 (2010) 5814–5819.
[25] H. Kurig, M. Vestli, K. Tõnurist, A. Jänes, E. Lust, J. Electrochem. Soc. 159 (2012) A944–A951.
[26] K. Yuyama, G. Masuda, H. Yoshida, T. Sato, J. Power Sources 162 (2006) 1401–1408.
[27] D.R. MacFarlane, N. Tachikawa, M. Forsyth, J.M. Pringle, P.C. Howlett, G.D. Elliott, J.H. Davis, M. Watanabe, P. Simon, C.A. Angell, Energy Environ. Sci. 7 (2014) 232–250.
[28] M. Galiński, A. Lewandowski, I. Stępniak, Electrochimica Acta 51 (2006) 5567–5580.
[29] S.A. Kislenko, I.S. Samoylov, R.H. Amirov, Phys. Chem. Chem. Phys. 11 (2009) 5584.
[30] R. Costa, C.M. Pereira, F. Silva, RSC Adv. 3 (2013) 11697–11706.
[31] Y. Su, J. Yan, M. Li, M. Zhang, B. Mao, J. Phys. Chem. C 117 (2013) 205–212.
[32] F. Endres, S.Z.E. Abedin, Phys. Chem. Chem. Phys. 8 (2006) 2101–2116.

[33] Y. Yokota, T. Harada, K. Fukui, Chem. Commun. 46 (2010) 8627–8629.
[34] A. Foelske-Schmitz, D. Weingarth, R. Kötz, Electrochimica Acta 56 (2011) 10321–10331.
[35] L. Siinor, J. Poom, C. Siimenson, K. Lust, E. Lust, J. Electroanal. Chem. 719 (2014) 133–137.
[36] M.V. Fedorov, A.A. Kornyshev, Chem. Rev. 114 (2014) 2978–3036.
[37] M.V. Fedorov, A.A. Kornyshev, Electrochimica Acta 53 (2008) 6835–6740.
[38] V. Ivaništšev, M.V. Fedorov, Electrochem. Soc. Interface 23 (2014) 65–69.
[39] R. Atkin, G.G. Warr, J. Phys. Chem. C 111 (2007) 5162–5168.
[40] A.M. Smith, K.R.J. Lovelock, N.N. Gosvami, P. Licence, A. Dolan, T. Welton, S. Perkin, J. Phys. Chem. Lett. 4 (2013) 378–382.
[41] S. Perkin, Phys. Chem. Chem. Phys. 14 (2012) 5052.
[42] J.M. Walls, Methods of Surface Analysis: Techniques and Applications, CUP Archive, 1990.
[43] D. Brune, R. Hellborg, H.J. Whitlow, O. Hunderi, Surface Characterization: A User's Sourcebook, John Wiley & Sons, 2008.
[44] A.A.J. Torriero, Electrochemistry in Ionic Liquids: Volume 1: Fundamentals, Springer, 2015.
[45] D.R. MacFarlane, M. Forsyth, P.C. Howlett, J.M. Pringle, J. Sun, G. Annat, W. Neil, E.I. Izgorodina, Acc. Chem. Res. 40 (2007) 1165–1173.
[46] T. Thomberg, T. Tooming, K. Liivand, L. Siinor, A. Jänes, E. Lust, in:, 2015, pp. 1–11.
[47] A. Lewandowski, A. Świderska-Mocek, J. Power Sources 194 (2009) 601–609.
[48] H. Kurig, M. Vestli, A. Jaenes, E. Lust, Electrochem. Solid State Lett. 14 (2011) A120–A122.
[49] R. Palm, H. Kurig, K. Tõnurist, A. Jänes, E. Lust, Electrochimica Acta 85 (2012) 139–144.
[50] S. Yamazaki, T. Ito, M. Yamagata, M. Ishikawa, Electrochimica Acta 86 (2012) 294–297.
[51] K.L. Van Aken, M. Beidaghi, Y. Gogotsi, Angew. Chem. Int. Ed. 54 (2015) 4806–4809.
[52] Z. Lei, Z. Liu, H. Wang, X. Sun, L. Lu, X.S. Zhao, J. Mater. Chem. A 1 (2013) 2313–2321.
[53] R. Lin, P.-L. Taberna, S. Fantini, V. Presser, C.R. Pérez, F. Malbosc, N.L. Rupesinghe, K.B.K. Teo, Y. Gogotsi, P. Simon, J. Phys. Chem. Lett. 2 (2011) 2396–2401.
[54] E. Frackowiak, G. Lota, J. Pernak, Appl. Phys. Lett. 86 (2005) 164104.
[55] E. Frackowiak, J. Braz. Chem. Soc. 17 (2006) 1074–1082.
[56] F. Moosavi, in:, J. Kadokawa (Ed.), Ion. Liq. – New Asp. Future, InTech, 2013.
[57] E. Bodo, V. Migliorati, in:, S. Handy (Ed.), Ion. Liq. – Cl. Prop., InTech, 2011.
[58] D.D. Macdonald, Electrochimica Acta 51 (2006) 1376–1388.
[59] J.F. Brennecke, E.J. Maginn, AIChE J. 47 (2001) 2384–2389.
[60] Y. Cao, T. Mu, Ind. Eng. Chem. Res. 53 (2014) 8651–8664.
[61] H. Ohno, Electrochemical Aspects of Ionic Liquids, John Wiley & Sons, 2011.
[62] A. Noda, K. Hayamizu, M. Watanabe, J. Phys. Chem. B 105 (2001) 4603–4610.
[63] S. Zhang, X. Lu, Q. Zhou, X. Li, X. Zhang, S. Li, Ionic Liquids: Physicochemical Properties, 1st ed., Elsevier Science, 2009.
[64] L.G. Sánchez, J.R. Espel, F. Onink, G.W. Meindersma, A.B. de Haan, J. Chem. Eng. Data 54 (2009) 2803–2812.

[65] K.N. Marsh, J.A. Boxall, R. Lichtenthaler, Fluid Phase Equilibria 219 (2004) 93–98.
[66] J.O. Bockris, A.K.N. Reddy, M. Gamboa-Aldeco, Modern Electrochemistry, 2nd ed., Kluwer Academic Publishers, New York, 2002.
[67] O.O. Okoturo, T.J. VanderNoot, J. Electroanal. Chem. 568 (2004) 167–181.
[68] C.M.A. Brett, A.M.O. Brett, Electrochemistry: Principles, Methods, and Applications, Oxford University Press, Incorporated, 1993.
[69] Y.-S. Liu, G.-B. P, in:, A. Kokorin (Ed.), Ion. Liq. Appl. Perspect., InTech, 2011.
[70] F. Endres, D. MacFarlane, A. Abbott, Electrodeposition from Ionic Liquids, John Wiley & Sons, 2008.
[71] M. Väärtnõu, E. Lust, Electrochimica Acta 47 (2001) 997–1005.
[72] E. Anderson, V. Grozovski, L. Siinor, C. Siimenson, E. Lust, J. Electroanal. Chem. 758 (2015) 201–208.
[73] T. Romann, O. Oll, P. Pikma, K. Kirsimäe, E. Lust, J. Power Sources 280 (2015) 606–611.
[74] J.P. Zheng, S.S. Moganty, P.C. Goonetilleke, R.E. Baltus, D. Roy, J. Phys. Chem. C 115 (2011) 7527–7537.
[75] S.S. Moganty, R.E. Baltus, D. Roy, Chem. Phys. Lett. 483 (2009) 90–94.
[76] H. Liu, Y. Liu, J. Li, Phys. Chem. Chem. Phys. 12 (2010) 1685–1697.
[77] M. Armand, F. Endres, D.R. MacFarlane, H. Ohno, B. Scrosati, Nat. Mater. 8 (2009) 621–629.
[78] A. Elbourne, S. McDonald, K. Voïchovsky, F. Endres, G.G. Warr, R. Atkin, ACS Nano 9 (2015) 7608–7620.
[79] W.-Y. Tsai, R. Lin, S. Murali, L. Li Zhang, J.K. McDonough, R.S. Ruoff, P.-L. Taberna, Y. Gogotsi, P. Simon, Nano Energy 2 (2013) 403–411.
[80] P. Hofmann, Prog. Surf. Sci. 81 (2006) 191–245.
[81] J. Wang, Electroanalysis 17 (2005) 1341–1346.
[82] Y. Li, M.A. Trujillo, E. Fu, B. Patterson, L. Fei, Y. Xu, S. Deng, S. Smirnov, H. Luo, J. Mater. Chem. A 1 (2013) 12123–12127.
[83] A.V. Ofitserov, V.S. Edel'man, J. Exp. Theor. Phys. 93 (2001) 642–648.
[84] H. Fei, Z. Feng, X. Liu, Ionics 21 (2014) 1967–1972.
[85] F. Ma, M. Zhou, Y. Jiao, G. Gao, Y. Gu, A. Bilic, Z. Chen, A. Du, Sci. Rep. 5 (2015) 17558.
[86] V. Ivaništšev, R.R. Nazmutdinov, E. Lust, Surf. Sci. 609 (2013) 91–99.
[87] A. Jänes, G. Nurk, K. Lust, J. Ehrlich, E. Lust, Russ. J. Electrochem. 38 (2002) 8–19.
[88] N. Margalit, Non-Aqueous Primary Battery Having a Bismuth (III) Sulfide Cathode, US4229509 A, 1980.
[89] R. Küchler, L. Steinke, R. Daou, M. Brando, K. Behnia, F. Steglich, Nat. Mater. 13 (2014) 461–465.
[90] N.M. Sammes, G.A. Tompsett, H. Näfe, F. Aldinger, J. Eur. Ceram. Soc. 19 (1999) 1801–1826.
[91] H. Mönig, J. Sun, Y.M. Koroteev, G. Bihlmayer, J. Wells, E.V. Chulkov, K. Pohl, P. Hofmann, Phys. Rev. B 72 (2005) 85410.
[92] S. Takaoka, H. Kawamura, K. Murase, S. Takano, Phys. Rev. B 13 (1976) 1428–1433.
[93] I. Švancara, C. Prior, S.B. Hočevar, J. Wang, Electroanalysis 22 (2010) 1405–1420.
[94] F. Jona, Surf. Sci. 8 (1967) 57–76.

[95] T. Romann, M. Väärtnou, A. Jänes, E. Lust, Electrochimica Acta 53 (2008) 8166–8171.
[96] K. Lust, M. Väärtnõu, E. Lust, J. Electroanal. Chem. 532 (2002) 303–318.
[97] C. Siimenson, L. Siinor, K. Lust, E. Lust, ECS Electrochem. Lett. 4 (2015) H62–H65.
[98] L. Siinor, Adsorption Kinetics of Ions at Bi Single Crystal Planes from Aqueous Electrolyte Solutions and Room-Temperature Ionic Liquids, University of Tartu, 2010.
[99] A. Wieckowski, Interfacial Electrochemistry: Theory: Experiment, and Applications, CRC Press, 1999.
[100] C.G. Zoski, Handbook of Electrochemistry, Elsevier, 2007.
[101] A.T. Hubbard, Encyclopedia of Surface and Colloid Science -, CRC Press, 2002.
[102] F. Endres, O. Höfft, N. Borisenko, L.H. Gasparotto, A. Prowald, R. Al-Salman, T. Carstens, R. Atkin, A. Bund, S.Z. El Abedin, Phys. Chem. Chem. Phys. 12 (2010) 1724–1732.
[103] T. Romann, O. Oll, P. Pikma, H. Tamme, E. Lust, Electrochimica Acta 125 (2014) 183–190.
[104] T. Leitner, J. Kattner, H. Hoffmann, Appl. Spectrosc. 57 (2003) 1502–1509.
[105] V. Ivaništšev, Double Layer Structure and Adsorption Kinetics of Ions at Metal Electrodes in Room Temperature Ionic Liquids, University of Tartu, 2012.
[106] K. Kirchner, T. Kirchner, V. Ivaništšev, M.V. Fedorov, Electrochimica Acta 110 (2013) 762–771.
[107] E. Anderson, V. Grozovski, L. Siinor, C. Siimenson, V. Ivaništšev, K. Lust, S. Kallip, E. Lust, J. Electroanal. Chem. 709 (2013) 46–56.
[108] C. Siimenson, L. Siinor, K. Lust, E. Lust, J. Electroanal. Chem. 730 (2014) 59–64.
[109] R. Atkin, S.Z. El Abedin, R. Hayes, L.H.S. Gasparotto, N. Borisenko, F. Endres, J. Phys. Chem. C 113 (2009) 13266–13272.
[110] Y.-Z. Su, Y.-C. Fu, Y.-M. Wei, J.-W. Yan, B.-W. Mao, ChemPhysChem 11 (2010) 2764–2778.
[111] F.G. Thomas, G. Henze, Introduction to Voltammetric Analysis: Theory and Practice, Csiro Publishing, 2001.
[112] R.S. Nicholson, Anal. Chem. 37 (1965) 1351–1355.
[113] J. Wang, Analytical Electrochemistry, John Wiley & Sons, 2006.
[114] P.T. Kissinger, W.R. Heineman, J. Chem. Educ. 60 (1983) 702.
[115] R.G. Compton, C.E. Banks, Understanding Voltammetry, World Scientific, 2011.
[116] A. Cuesta, A. Couto, A. Rincón, M.C. Pérez, A. López-Cudero, C. Gutiérrez, J. Electroanal. Chem. 586 (2006) 184–195.
[117] M. Freemantle, An Introduction to Ionic Liquids, Royal Society of Chemistry, 2010.
[118] M. György Inzelt, Andrzej Lewenstam, Fritz Scholz, eds., Handbook of Reference Electrodes, Springer-Verlag Berlin Heidelberg, New York, 2013.
[119] E. Barsoukov, J.R. Macdonald, Impedance Spectroscopy: Theory, Experiment, and Applications, Wiley, John & Sons, Incorporated, 2005.
[120] A.J. Bard, M. Stratmann, P.R. Unwin, eds., Encyclopedia of Electrochemistry: Instrumentation and Electroanalytical Chemistry v. 3, Wiley VCH, 2003.
[121] A.J. Bard, L.R. Faulkner, Electrochemical Methods: Fundamentals and Applications, Wiley, 2000.

[122] V.F. Lvovich, Impedance Spectroscopy: Applications to Electrochemical and Dielectric Phenomena, John Wiley & Sons, 2012.
[123] M.-G. Olivier, M. Poelm, in:, R. Shoja Razavi (Ed.), Recent Res. Corros. Eval. Prot., InTech, 2012.
[124] M.E. Orazem, B. Tribollet, Electrochemical Impedance Spectroscopy, John Wiley & Sons, 2011.
[125] X.-Z.R. Yuan, C. Song, H. Wang, J. Zhang, Electrochemical Impedance Spectroscopy in PEM Fuel Cells: Fundamentals and Applications, Springer Science & Business Media, 2009.
[126] C. Nanjundiah, S.F. McDevitt, V.R. Koch, J. Electrochem. Soc. 144 (1997) 3392–3397.
[127] V. Lockett, M. Horne, R. Sedev, T. Rodopoulos, J. Ralston, Phys. Chem. Chem. Phys. 12 (2010) 12499–12512.
[128] G.A. Martynov, R.R. Salem, Electrical Double Layer at a Metal-Dilute Electrolyte Solution Interface, Springer Science & Business Media, 2012.
[129] M.V. Fedorov, N. Georgi, A.A. Kornyshev, Electrochem. Commun. 12 (2010) 296–299.
[130] M.Z. Bazant, B.D. Storey, A.A. Kornyshev, Phys. Rev. Lett. 106 (2011) 46102–4.
[131] C. Merlet, D.T. Limmer, M. Salanne, R. van Roij, P.A. Madden, D. Chandler, B. Rotenberg, J. Phys. Chem. C 118 (2014) 18291–18298.
[132] Y. Lauw, M.D. Horne, T. Rodopoulos, A. Nelson, F.A.M. Leermakers, J. Phys. Chem. B 114 (2010) 11149–11154.
[133] A.A. Kornyshev, J. Phys. Chem. B 111 (2007) 5545–5557.
[134] A.A. Kornyshev, N.B. Luque, W. Schmickler, J. Solid State Electrochem. 18 (2014) 1345–1349.
[135] K.B. Oldham, J. Electroanal. Chem. 613 (2008) 131–138.
[136] B. Skinner, M.S. Loth, B.I. Shklovskii, Phys. Rev. Lett. 104 (2010) 128302–4.
[137] M.S. Loth, B. Skinner, B.I. Shklovskii, Phys. Rev. E 82 (2010) 16107–16.
[138] L. del Olmo, R. López, J.M. García de la Vega, Int. J. Quantum Chem. 113 (2013) 852–858.
[139] K. Lee, Y. Morikawa, D.C. Langreth, Phys. Rev. B 82 (2010).
[140] V. Ivaništšev, A. Ruzanov, K. Lust, E. Lust, J. Electrochem. Soc. 160 (2013) H368–H375.
[141] V. Ivaništšev, S. O'Connor, M.V. Fedorov, Electrochem. Commun. 48 (2014) 61–64.
[142] V. Ivaništšev, K. Kirchner, T. Kirchner, M.V. Fedorov, J. Phys. Condens. Matter 27 (2015) 102101.
[143] T. Carstens, A. Ispas, N. Borisenko, R. Atkin, A. Bund, F. Endres, Electrochimica Acta (n.d.).
[144] L. Yu, Y. Huang, X. Jin, A.J. Mason, X. Zeng, Sens. Actuators B Chem. 140 (2009) 363–370.
[145] N. Borisenko, A. Ispas, E. Zschippang, Q. Liu, S. Zein El Abedin, A. Bund, F. Endres, Electrochimica Acta 54 (2009) 1519–1528.
[146] E. Anderson, V. Grozovski, L. Siinor, C. Siimenson, E. Lust, Electrochem. Commun. 46 (2014) 18–21.
[147] S. Vanderaspoilden, J. Christophe, T. Doneux, C. Buess-Herman, Electrochimica Acta 162 (2015) 156–162.
[148] L. Siinor, K. Lust, E. Lust, J. Electroanal. Chem. 601 (2007) 39–46.

[149] L. Siinor, V. Ivaništšev, K. Lust, E. Lust, J. Solid State Electrochem. 14 (2010) 555–563.
[150] M. Väärtnõu, E. Lust, J. Solid State Electrochem. 18 (2014) 173–180.
[151] M. Väärtnõu, E. Lust, J. Electroanal. Chem. 733 (2014) 20–26.
[152] K. Lust, E. Lust, J. Electroanal. Chem. 552 (2003) 129–139.
[153] L. Siinor, K. Lust, E. Lust, ECS Trans. 16 (2009) 559.
[154] L. Siinor, K. Lust, E. Lust, J. Electrochem. Soc. 157 (2010) F83–F87.
[155] L. Siinor, K. Lust, E. Lust, Electrochem. Commun. 12 (2010) 1058–1061.
[156] E. Frackowiak, M. Meller, J. Menzel, D. Gastol, K. Fic, Faraday Discuss (2014).
[157] L. Siinor, C. Siimenson, V. Ivaništšev, K. Lust, E. Lust, J. Electroanal. Chem. 668 (2012) 30–36.
[158] M. Väärtnõu, E. Lust, J. Electroanal. Chem. 565 (2004) 211–218.
[159] T. Tooming, T. Thomberg, L. Siinor, K. Tõnurist, A. Jänes, E. Lust, J. Electrochem. Soc. 161 (2014) A222–A227.
[160] J. Eskusson, A. Jänes, A. Kikas, L. Matisen, E. Lust, J. Power Sources 196 (2011) 4109–4116.
[161] G.D. Allen, M.C. Buzzeo, C. Villagrán, C. Hardacre, R.G. Compton, J. Electroanal. Chem. 575 (2005) 311–320.
[162] H. Ashassi-Sorkhabi, M. Es'haghi, Mater. Chem. Phys. 114 (2009) 267–271.
[163] X. Yang, L. He, S. Qin, G.-H. Tao, M. Huang, Y. Lv, PLoS ONE 9 (2014) e95832.
[164] T. Iwasita, M.C. Giordano, Electrochimica Acta 14 (1969) 1045–1059.
[165] A. Efimova, L. Pfützner, P. Schmidt, Thermochim. Acta 604 (2015) 129–136.
[166] G.D. Allen, M.C. Buzzeo, C. Villagrán, C. Hardacre, R.G. Compton, J. Electroanal. Chem. 575 (2005) 311–320.
[167] A.M. O'Mahony, D.S. Silvester, L. Aldous, C. Hardacre, R.G. Compton, J. Chem. Eng. Data 53 (2008) 2884–2891.
[168] A. Lasia, in:, Mod. Asp. Electrochem., Springer, 2002, pp. 143–248.
[169] F. Beguin, E. Frackowiak, Supercapacitors: Materials, Systems and Applications, John Wiley & Sons, 2013.
[170] K. Tõnurist, T. Thomberg, A. Jänes, I. Kink, E. Lust, Electrochem. Commun. 22 (2012) 77–80.
[171] J. Lipkowski, Z. Shi, A. Chen, B. Pettinger, C. Bilger, Electrochimica Acta 43 (1998) 2875–2888.
[172] A. Cuesta, D.M. Kolb, Surf. Sci. 465 (2000) 310–316.
[173] O.M. Magnussen, B.M. Ocko, J.X. Wang, R.R. Adzic, J. Phys. Chem. 100 (1996) 5500–5508.
[174] J.-F. Liu, W.A. Ducker, J. Phys. Chem. B 103 (1999) 8558–8567.
[175] H.W. Lei, H. Uchida, M. Watanabe, Langmuir 13 (1997) 3523–3528.
[176] J. Inukai, Y. Osawa, K. Itaya, J. Phys. Chem. B 102 (1998) 10034–10040.
[177] H. Matsumoto, J. Inukai, M. Ito, J. Electroanal. Chem. 379 (1994) 223–231.
[178] T. Teshima, K. Ogaki, K. Itaya, J. Phys. Chem. B 101 (1997) 2046–2053.

SUMMARY IN ESTONIAN

Halogeniid ioonide adsorptsiooni elektrokeemiline karakteriseerimine ioonsete vedelike segudes Bi(111) ja PG elektroodide piirpinnale

Uuetüübiliste energia salvestus- ja genereerimisseadmete jaoks on vaja välja töötada odavamaid ja keskkonnasõbralikumaid elektrolüüte. Ioonsete vedelike kasutamine elektrolüütidena võimaldab saavutada seadmete pikemat eluiga ning kõrgemat energia- ja võimsustihedust. Parimate omadustega elektrolüütide disainimiseks on väga oluline mõista faaside vahelistel piirpindadel toimuvate elektrokeemiliste protsesside seaduspärasusi.

Käesolevas töös uuriti faasidevahelistel piirpindadel toimuvaid protsesse järgmistes süsteemides: Bi(111)|EMImBF$_4$ + x% EMImI, Bi(111)|EMImBF$_4$ + EMImOTF + 1% EMImI, Bi(111)|EMImBF$_4$ + EMImBr, PG|EMImBF$_4$ + 5% EMImI (PG – pürolüütiline gtafiit). Elektrokeemiliseks karakteriseerimiseks kasutati tsüklilise voltamperomeetria ja elektrokeemilise impedantsspektroskoopia meetodeid. Mõõtmised näitasid, et antud elektrolüütide segusid on võimalik kasutada järgmistes tööelektroodi potentsiaalide vahemikes (ΔE): Bi(111) elektroodi puhul $\Delta E \approx 0.7\text{V}–1.2\text{V}$ ja PG puhul $\Delta E \approx 3\text{V}$. Vismutelektroodi kitsam potentsiaalide vahemik võrreldes süsinikelektroodiga tuleneb tema pinna elekrokeemilisest oksüdeerumisest positiivsematel elektroodi potentsiaalidel. Tihedusfuntsionaali teooria arvutusi ja *in situ* skaneeriva tunnelmikroskoopia tulemusi kasutati elektrokeemilistel mõõtmistel saadud tulemuste kinnitamiseks.

Leiti, et mahtuvuse maksimaalse väärtuse erinevus Br^- ja I^- sisaldavates elektrolüütide segude vahel on väiksem kui Bi(111) elektroodil vesilahuste korral. Samuti ennustas arvutuskeemia, et erinevus I^- ja Br^- adsorptsiooni vahel Bi ja süsinik elektroodil on väga väikesed, näidates seega head kooskõla eksperimentaalse ja teoreetilise arvutuskeemia tulemuste vahel. Mõõdetud süsteemid näitasid head ajalist stabiilsust ning olid antud potentsiaalide vahemikes elektrokeemiliselt pöörduvad, mis on võtmerolliks elektrolüüdi kasutamisel uuetüübilistes energiasalvestusseadmetes. Mahtuvuse väärtused kasvasid oluliselt halogeniid ioonide lisamisel lahusesse nende spetsiifilise adsorptsiooni tõttu vähem negatiivsematel potentsiaalidel. Adsorptsiooni olemasolu kinnitavad elektrokeemilise impedantsspektroskoopia andmed, näidates kõrgeid faasinurga väärtusi I^- ja Br^- lisandi korral, mis vastavad adsoprtsioonlimiteeritud protsessidele.

Leiti, et Bi(111) elektrood sobib ideaalselt fundamentaalseteks uuringuteks ning seda saab edukalt kasutada mudelsüsteemina, kui eesmärgiks on uuritavaid elektrolüüte rakendada tulevikus süsinikmaterialidel baseeruvates süsteemides. Seda tõestavad edukad katsed PG elektroodil ja D-glükoosist sünteesitud süsinikmaterjalil põhinevates kondensaatorites. Kasutades jodiidioone sisaldava ioonse vedeliku segusid elektrolüüdina saadi tulemuseks ligi 50% kõrgemad

mahtuvuse väärtused kui puhta $EMImBF_4$ korral. Head tulemused Bi ja süsinikmaterjalidel mõõdetud jodiid ioonide segude korral annab alust arvata, et ka bromiid ioone sisaldavad lahused sobivad kasutamiseks superkondensaatroites kõrgemate energia ja võimsustiheduste saavutamiseks. Elektrokeemiliste mõõtmiste tulemused on heas kooskõlas arvutsmeetodite ja pinnauuringute tulemustega ning seega võimaldades arendada edasi mudelid faaside vaheliste piirpindade iseloomustamiseks ja seda eriti selliste keeruliste süsteemide korral kui esineb spetsiifiline anioonide adsorptsioon.

ACKNOWLEDGEMENTS

First of all, I would like to express my greatest gratitude to my supervisors. Professor Enn Lust for scientific guidance and support during the time of my studies. Ph.D. Liis Siinor for her patience, guidance, inspiring ideas, interesting discussions and for the time invested in me.

I am very thankful to my family, especially to my mom, for their support and encouragement during my studies. I am deeply grateful to my friends, who have been there for me through good and bad times.

Thanks to all my colleagues for their support, advice and for creating an inspiring working atmosphere. Special thanks to Rait Kanarbik for the technical advice during my studies, Ove Oll and Vladislav Ivaništšev for theoretical advice.

The present study was performed at University of Tartu, Institute of Chemistry and was financially supported by Estonian Science Foundation Grants 7791, 8357 and 8786, PUT55, PUT1033, PUT1107. Estonian Energy Technology Program Project SLOKT10209T, Estonian Institutional Research Project IUT20-13, graduate School ‘‘Functional Materials and Technologies’’ receiving funding from the European Social Fund under Project 1.2.0401.09-0079 in Estonia and by the EU through the European Regional Development Fund (Estonian Centre of Excellence in Science projects: 3.2.0101–0030 and 2014-2020.4.01.15-0011).

PUBLICATIONS

CURRICULUM VITAE

Name: Carolin Siimenson
Date of birth: December 3, 1988
Citizenship: Estonian
Contact: Institute of Chemistry, University of Tartu
Ravila 14a, 50411, Tartu, Estonia
E-mail: carolinsiimenson@gmail.com

Education:

2012–…	University of Tartu, Institute of Chemistry, PhD student
2010–2012	University of Tartu – Master's degree in chemistry
2007–2010	University of Tartu – Bachelor degree in chemistry

Professional Employment:

2010–…	University of Tartu, Institute of Chemistry, Chemist

List of publications:

1. L. Siinor, C. Siimenson, V. Ivanistsev, K. Lust, E. Lust, Influence of cation chemical composition and structure on the double layer capacitance for Bi(111)|room temperature ionic liquid interface. Journal of Electroanalytical Chemistry, 688 (2012) 30–36.
2. C. Siimenson, J. Kruusma, E. Anderson, M. Merisalu, V. Sammelselg, E. Lust, C. B. Banks, Prussian blue modified solid carbon nanorod whisker paste composite electrodes: Evaluation towards the electroanalytical sensing of H2O2. International Jornal of Electrochemistry, 2012 (2012) 7
3. L. Siinor, C. Siimenson, K. Lust, E. Lust, Mixture of 1-ethyl-3-methyl-imidazolium tetrafluoroborate and 1-ethyl-3-methylimidazolium iodide: A new potential high capacitance electrolyte for EDLCs. Electrochemistry Communications, 35 (2013) 5–7.
4. E. Anderson, V. Grozovski, L. Siinor, C. Siimenson, V. Ivaništšev, K. Lust, S. Kallip. E. Lust, Influence of the electrode potential and in situ STM scanning conditions on the phase boundary structure of the single crystal Bi(111)|1-butyl-4-methylpyridinium tetrafluoroborate interface. Journal of Electroanalytical Chemistry, 709 (2013) 46–56
5. L. Siinor, J. Poom, C.Siimenson, K. Lust, E. Lust, Electrochemical characteristics pyrolytic graphitelmixture of 1-ethyl-3-methylimidazolium tetrafluoroborate and 1-ethyl-3-methylimidazolium iodide interface. Journal of Electroanalytical Chemistry, 719 (2014) 133–137.
6. E. Anderson, V. Grozovski, L. Siinor, C. Siimenson, E. Lust, In situ STM studies of Bi(111)|1.ethyl-3-methylimidazolium tetrafluoroborate + 1-ethyl-3-methylimidazolium iodide interface. Electrochemistry Communications, 46 (2014) 18–21

7. C. Siimenson, L. Siinor, K. Lust, E. Lust, The electrochemical characteristics of the mixture of 1-ethyl-3-methylimidazolium tetrafluoroborate and 1-ethyl-3-methylimidazolium iodide. Journal of Electroanalytical Chemistry, 730 (2014) 59–64.
8. C. Siimenson, L. Siinor, K. Lust, E. Lust, Electrochemical Characterization of Iodide Ions Adsorption kinetics at Bi(111) Electrode from Three-Component Ionic Liquids Mixtures. ECS Electrochemistry Letters, (2015) 4 (12), H1−H4.
9. E. Anderson, V. Grozovski, L. Siinor, C. Siimenson, E. Lust, Comparative in situ STM, cyclic voltammetry and impedance spectroscopy study of Bi(111) | 1-ethyl-3-methylimidazolium tetrafluoroborate interface. Journal of Electroanalytical Chemistry, 758 (2015) 201–208.
10. **C. Siimenson**, M. Lembinen, O. Oll, L. Läll, M. Tarkanovskaja, V. Ivaništšev, L. Siinor,. T. Thomberg, K. Lust, E. Lust, Electrochemical investigation of 1-ethyl-3-methylimidazolium bromide and tetrafluoroborate mixture at Bi(111) electrode interface. Joural of The Electochemical Society, 163 (2016) H723-H730

ELULOOKIRJELDUS

Nimi: Carolin Siimenson
Sünniaeg: 3. detsember 1988
Kodakondsus: Eesti
kontakt: Keemia Instituut, Tartu Ülikool
Ravila 14a, 50411, Tartu, Eesti
E-post: carolinsiimenson@gmail.com

Haridus:

2012–…	Tartu Ülikool, Keemia Instituut, doktorant
2010–2012	Tartu Ülikool – Magistrikraad keemias
2007–2010	Tartu Ülikool – Bakalaureusekraad keemias

Teenistuskäik:

2010–…	Tartu Ülikool, Keemia Instituut, keemik

Teaduspublikatsioonid:

1. L. Siinor, **C**. Siimenson, V. Ivanistsev, K. Lust, E. Lust, Influence of cation chemical composition and structure on the double layer capacitance for Bi(111)|room temperature ionic liquid interface. Journal of Electroanalytical Chemistry, 688 (2012) 30–36.
2. C. Siimenson, J. Kruusma, E. Anderson, M. Merisalu, V. Sammelselg, E. Lust, C. B. Banks, Prussian blue modified solid carbon nanorod whisker paste composite electrodes: Evaluation towards the electroanalytical sensing of H2O2. International Jornal of Electrochemistry, 2012 (2012) 7
3. L. Siinor, C. Siimenson, K. Lust, E. Lust, Mixture of 1-ethyl-3-methylimidazolium tetrafluoroborate and 1-ethyl-3-methylimidazolium iodide: A new potential high capacitance electrolyte for EDLCs. Electrochemistry Communications, 35 (2013) 5–7.
4. E. Anderson, V. Grozovski, L. Siinor, C. Siimenson, V. Ivaništšev, K. Lust, S. Kallip. E. Lust, Influence of the electrode potential and in situ STM scanning conditions on the phase boundary structure of the single crystal Bi(111)|1-butyl-4-methylpyridinium tetrafluoroborate interface. Journal of Electroanalytical Chemistry, 709 (2013) 46–56
5. L. Siinor, J. Poom, C. Siimenson, K. Lust, E. Lust, Electrochemical characteristics pyrolytic graphitelmixture of 1-ethyl-3-methylimidazolium tetrafluoroborate and 1-ethyl-3-methylimidazolium iodide interface. Journal of Electroanalytical Chemistry, 719 (2014) 133–137.
6. E. Anderson, V. Grozovski, L. Siinor, C. Siimenson, E. Lust, In situ STM studies of Bi(111)|1.ethyl-3-methylimidazolium tetrafluoroborate + 1-ethyl-3-methylimidazolium iodide interface. Electrochemistry Communications, 46 (2014) 18–21

7. C. Siimenson, L. Siinor, K. Lust, E. Lust, The electrochemical characteristics of the mixture of 1-ethyl-3-methylimidazolium tetrafluoroborate and 1-ethyl-3-methylimidazolium iodide. Journal of Electroanalytical Chemistry, 730 (2014) 59–64.
8. C. Siimenson, L. Siinor, K. Lust, E. Lust, Electrochemical Characterization of Iodide Ions Adsorption kinetics at Bi(111) Electrode from Three-Component Ionic Liquids Mixtures. ECS Electrochemistry Letters, (2015) 4 (12), H1−H4.
9. E. Anderson, V. Grozovski, L. Siinor, C. Siimenson, E. Lust, Comparative in situ STM, cyclic voltammetry and impedance spectroscopy study of Bi(111) | 1-ethyl-3-methylimidazolium tetrafluoroborate interface. Journal of Electroanalytical Chemistry, 758 (2015) 201–208.
10. **C. Siimenson**, M. Lembinen, O. Oll, L. Läll, M. Tarkanovskaja, V. Ivaništšev, L. Siinor,. T. Thomberg, K. Lust, E. Lust, Electrochemical investigation of 1-ethyl-3-methylimidazolium bromide and tetrafluoroborate mixture at Bi(111) electrode interface. Joural of The Electochemical Society, 163 (2016) H723-H730

DISSERTATIONES CHIMICAE UNIVERSITATIS TARTUENSIS

1. **Toomas Tamm.** Quantum-chemical simulation of solvent effects. Tartu, 1993, 110 p.
2. **Peeter Burk.** Theoretical study of gas-phase acid-base equilibria. Tartu, 1994, 96 p.
3. **Victor Lobanov.** Quantitative structure-property relationships in large descriptor spaces. Tartu, 1995, 135 p.
4. **Vahur Mäemets.** The ^{17}O and ^{1}H nuclear magnetic resonance study of H_2O in individual solvents and its charged clusters in aqueous solutions of electrolytes. Tartu, 1997, 140 p.
5. **Andrus Metsala.** Microcanonical rate constant in nonequilibrium distribution of vibrational energy and in restricted intramolecular vibrational energy redistribution on the basis of slater's theory of unimolecular reactions. Tartu, 1997, 150 p.
6. **Uko Maran.** Quantum-mechanical study of potential energy surfaces in different environments. Tartu, 1997, 137 p.
7. **Alar Jänes.** Adsorption of organic compounds on antimony, bismuth and cadmium electrodes. Tartu, 1998, 219 p.
8. **Kaido Tammeveski.** Oxygen electroreduction on thin platinum films and the electrochemical detection of superoxide anion. Tartu, 1998, 139 p.
9. **Ivo Leito.** Studies of Brønsted acid-base equilibria in water and non-aqueous media. Tartu, 1998, 101 p.
10. **Jaan Leis.** Conformational dynamics and equilibria in amides. Tartu, 1998, 131 p.
11. **Toonika Rinken.** The modelling of amperometric biosensors based on oxidoreductases. Tartu, 2000, 108 p.
12. **Dmitri Panov.** Partially solvated Grignard reagents. Tartu, 2000, 64 p.
13. **Kaja Orupõld.** Treatment and analysis of phenolic wastewater with microorganisms. Tartu, 2000, 123 p.
14. **Jüri Ivask.** Ion Chromatographic determination of major anions and cations in polar ice core. Tartu, 2000, 85 p.
15. **Lauri Vares.** Stereoselective Synthesis of Tetrahydrofuran and Tetrahydropyran Derivatives by Use of Asymmetric Horner-Wadsworth-Emmons and Ring Closure Reactions. Tartu, 2000, 184 p.
16. **Martin Lepiku.** Kinetic aspects of dopamine D_2 receptor interactions with specific ligands. Tartu, 2000, 81 p.
17. **Katrin Sak.** Some aspects of ligand specificity of P2Y receptors. Tartu, 2000, 106 p.
18. **Vello Pällin.** The role of solvation in the formation of iotsitch complexes. Tartu, 2001, 95 p.
19. **Katrin Kollist.** Interactions between polycyclic aromatic compounds and humic substances. Tartu, 2001, 93 p.

20. **Ivar Koppel.** Quantum chemical study of acidity of strong and superstrong Brønsted acids. Tartu, 2001, 104 p.
21. **Viljar Pihl.** The study of the substituent and solvent effects on the acidity of OH and CH acids. Tartu, 2001, 132 p.
22. **Natalia Palm.** Specification of the minimum, sufficient and significant set of descriptors for general description of solvent effects. Tartu, 2001, 134 p.
23. **Sulev Sild.** QSPR/QSAR approaches for complex molecular systems. Tartu, 2001, 134 p.
24. **Ruslan Petrukhin.** Industrial applications of the quantitative structure-property relationships. Tartu, 2001, 162 p.
25. **Boris V. Rogovoy.** Synthesis of (benzotriazolyl)carboximidamides and their application in relations with *N*- and *S*-nucleophyles. Tartu, 2002, 84 p.
26. **Koit Herodes.** Solvent effects on UV-vis absorption spectra of some solvatochromic substances in binary solvent mixtures: the preferential solvation model. Tartu, 2002, 102 p.
27. **Anti Perkson.** Synthesis and characterisation of nanostructured carbon. Tartu, 2002, 152 p.
28. **Ivari Kaljurand.** Self-consistent acidity scales of neutral and cationic Brønsted acids in acetonitrile and tetrahydrofuran. Tartu, 2003, 108 p.
29. **Karmen Lust.** Adsorption of anions on bismuth single crystal electrodes. Tartu, 2003, 128 p.
30. **Mare Piirsalu.** Substituent, temperature and solvent effects on the alkaline hydrolysis of substituted phenyl and alkyl esters of benzoic acid. Tartu, 2003, 156 p.
31. **Meeri Sassian.** Reactions of partially solvated Grignard reagents. Tartu, 2003, 78 p.
32. **Tarmo Tamm.** Quantum chemical modelling of polypyrrole. Tartu, 2003. 100 p.
33. **Erik Teinemaa.** The environmental fate of the particulate matter and organic pollutants from an oil shale power plant. Tartu, 2003. 102 p.
34. **Jaana Tammiku-Taul.** Quantum chemical study of the properties of Grignard reagents. Tartu, 2003. 120 p.
35. **Andre Lomaka.** Biomedical applications of predictive computational chemistry. Tartu, 2003. 132 p.
36. **Kostyantyn Kirichenko.** Benzotriazole – Mediated Carbon–Carbon Bond Formation. Tartu, 2003. 132 p.
37. **Gunnar Nurk.** Adsorption kinetics of some organic compounds on bismuth single crystal electrodes. Tartu, 2003, 170 p.
38. **Mati Arulepp.** Electrochemical characteristics of porous carbon materials and electrical double layer capacitors. Tartu, 2003, 196 p.
39. **Dan Cornel Fara.** QSPR modeling of complexation and distribution of organic compounds. Tartu, 2004, 126 p.
40. **Riina Mahlapuu.** Signalling of galanin and amyloid precursor protein through adenylate cyclase. Tartu, 2004, 124 p.

41. **Mihkel Kerikmäe.** Some luminescent materials for dosimetric applications and physical research. Tartu, 2004, 143 p.
42. **Jaanus Kruusma.** Determination of some important trace metal ions in human blood. Tartu, 2004, 115 p.
43. **Urmas Johanson.** Investigations of the electrochemical properties of polypyrrole modified electrodes. Tartu, 2004, 91 p.
44. **Kaido Sillar.** Computational study of the acid sites in zeolite ZSM-5. Tartu, 2004, 80 p.
45. **Aldo Oras.** Kinetic aspects of dATPαS interaction with $P2Y_1$ receptor. Tartu, 2004, 75 p.
46. **Erik Mölder.** Measurement of the oxygen mass transfer through the air-water interface. Tartu, 2005, 73 p.
47. **Thomas Thomberg.** The kinetics of electroreduction of peroxodisulfate anion on cadmium (0001) single crystal electrode. Tartu, 2005, 95 p.
48. **Olavi Loog.** Aspects of condensations of carbonyl compounds and their imine analogues. Tartu, 2005, 83 p.
49. **Siim Salmar.** Effect of ultrasound on ester hydrolysis in aqueous ethanol. Tartu, 2006, 73 p.
50. **Ain Uustare.** Modulation of signal transduction of heptahelical receptors by other receptors and G proteins. Tartu, 2006, 121 p.
51. **Sergei Yurchenko.** Determination of some carcinogenic contaminants in food. Tartu, 2006, 143 p.
52. **Kaido Tämm.** QSPR modeling of some properties of organic compounds. Tartu, 2006, 67 p.
53. **Olga Tšubrik.** New methods in the synthesis of multisubstituted hydrazines. Tartu. 2006, 183 p.
54. **Lilli Sooväli.** Spectrophotometric measurements and their uncertainty in chemical analysis and dissociation constant measurements. Tartu, 2006, 125 p.
55. **Eve Koort.** Uncertainty estimation of potentiometrically measured ph and pK_a values. Tartu, 2006, 139 p.
56. **Sergei Kopanchuk.** Regulation of ligand binding to melanocortin receptor subtypes. Tartu, 2006, 119 p.
57. **Silvar Kallip.** Surface structure of some bismuth and antimony single crystal electrodes. Tartu, 2006, 107 p.
58. **Kristjan Saal.** Surface silanization and its application in biomolecule coupling. Tartu, 2006, 77 p.
59. **Tanel Tätte.** High viscosity $Sn(OBu)_4$ oligomeric concentrates and their applications in technology. Tartu, 2006, 91 p.
60. **Dimitar Atanasov Dobchev**. Robust QSAR methods for the prediction of properties from molecular structure. Tartu, 2006, 118 p.
61. **Hannes Hagu**. Impact of ultrasound on hydrophobic interactions in solutions. Tartu, 2007, 81 p.

62. **Rutha Jäger.** Electroreduction of peroxodisulfate anion on bismuth electrodes. Tartu, 2007, 142 p.
63. **Kaido Viht.** Immobilizable bisubstrate-analogue inhibitors of basophilic protein kinases: development and application in biosensors. Tartu, 2007, 88 p.
64. **Eva-Ingrid Rõõm.** Acid-base equilibria in nonpolar media. Tartu, 2007, 156 p.
65. **Sven Tamp.** DFT study of the cesium cation containing complexes relevant to the cesium cation binding by the humic acids. Tartu, 2007, 102 p.
66. **Jaak Nerut.** Electroreduction of hexacyanoferrate(III) anion on Cadmium (0001) single crystal electrode. Tartu, 2007, 180 p.
67. **Lauri Jalukse.** Measurement uncertainty estimation in amperometric dissolved oxygen concentration measurement. Tartu, 2007, 112 p.
68. **Aime Lust.** Charge state of dopants and ordered clusters formation in CaF_2:Mn and CaF_2:Eu luminophors. Tartu, 2007, 100 p.
69. **Iiris Kahn**. Quantitative Structure-Activity Relationships of environmentally relevant properties. Tartu, 2007, 98 p.
70. **Mari Reinik.** Nitrates, nitrites, N-nitrosamines and polycyclic aromatic hydrocarbons in food: analytical methods, occurrence and dietary intake. Tartu, 2007, 172 p.
71. **Heili Kasuk.** Thermodynamic parameters and adsorption kinetics of organic compounds forming the compact adsorption layer at Bi single crystal electrodes. Tartu, 2007, 212 p.
72. **Erki Enkvist.** Synthesis of adenosine-peptide conjugates for biological applications. Tartu, 2007, 114 p.
73. **Svetoslav Hristov Slavov**. Biomedical applications of the QSAR approach. Tartu, 2007, 146 p.
74. **Eneli Härk.** Electroreduction of complex cations on electrochemically polished Bi(*hkl*) single crystal electrodes. Tartu, 2008, 158 p.
75. **Priit Möller.** Electrochemical characteristics of some cathodes for medium temperature solid oxide fuel cells, synthesized by solid state reaction technique. Tartu, 2008, 90 p.
76. **Signe Viggor.** Impact of biochemical parameters of genetically different pseudomonads at the degradation of phenolic compounds. Tartu, 2008, 122 p.
77. **Ave Sarapuu.** Electrochemical reduction of oxygen on quinone-modified carbon electrodes and on thin films of platinum and gold. Tartu, 2008, 134 p.
78. **Agnes Kütt.** Studies of acid-base equilibria in non-aqueous media. Tartu, 2008, 198 p.
79. **Rouvim Kadis.** Evaluation of measurement uncertainty in analytical chemistry: related concepts and some points of misinterpretation. Tartu, 2008, 118 p.
80. **Valter Reedo.** Elaboration of IVB group metal oxide structures and their possible applications. Tartu, 2008, 98 p.

81. **Aleksei Kuznetsov.** Allosteric effects in reactions catalyzed by the cAMP-dependent protein kinase catalytic subunit. Tartu, 2009, 133 p.
82. **Aleksei Bredihhin.** Use of mono- and polyanions in the synthesis of multisubstituted hydrazine derivatives. Tartu, 2009, 105 p.
83. **Anu Ploom.** Quantitative structure-reactivity analysis in organosilicon chemistry. Tartu, 2009, 99 p.
84. **Argo Vonk.** Determination of adenosine A_{2A}- and dopamine D_1 receptor-specific modulation of adenylate cyclase activity in rat striatum. Tartu, 2009, 129 p.
85. **Indrek Kivi.** Synthesis and electrochemical characterization of porous cathode materials for intermediate temperature solid oxide fuel cells. Tartu, 2009, 177 p.
86. **Jaanus Eskusson.** Synthesis and characterisation of diamond-like carbon thin films prepared by pulsed laser deposition method. Tartu, 2009, 117 p.
87. **Marko Lätt.** Carbide derived microporous carbon and electrical double layer capacitors. Tartu, 2009, 107 p.
88. **Vladimir Stepanov.** Slow conformational changes in dopamine transporter interaction with its ligands. Tartu, 2009, 103 p.
89. **Aleksander Trummal.** Computational Study of Structural and Solvent Effects on Acidities of Some Brønsted Acids. Tartu, 2009, 103 p.
90. **Eerold Vellemäe.** Applications of mischmetal in organic synthesis. Tartu, 2009, 93 p.
91. **Sven Parkel.** Ligand binding to 5-HT_{1A} receptors and its regulation by Mg^{2+} and Mn^{2+}. Tartu, 2010, 99 p.
92. **Signe Vahur.** Expanding the possibilities of ATR-FT-IR spectroscopy in determination of inorganic pigments. Tartu, 2010, 184 p.
93. **Tavo Romann**. Preparation and surface modification of bismuth thin film, porous, and microelectrodes. Tartu, 2010, 155 p.
94. **Nadežda Aleksejeva.** Electrocatalytic reduction of oxygen on carbon nanotube-based nanocomposite materials. Tartu, 2010, 147 p.
95. **Marko Kullapere.** Electrochemical properties of glassy carbon, nickel and gold electrodes modified with aryl groups. Tartu, 2010, 233 p.
96. **Liis Siinor.** Adsorption kinetics of ions at Bi single crystal planes from aqueous electrolyte solutions and room-temperature ionic liquids. Tartu, 2010, 101 p.
97. **Angela Vaasa.** Development of fluorescence-based kinetic and binding assays for characterization of protein kinases and their inhibitors. Tartu 2010, 101 p.
98. **Indrek Tulp.** Multivariate analysis of chemical and biological properties. Tartu 2010, 105 p.
99. **Aare Selberg.** Evaluation of environmental quality in Northern Estonia by the analysis of leachate. Tartu 2010, 117 p.
100. **Darja Lavõgina.** Development of protein kinase inhibitors based on adenosine analogue-oligoarginine conjugates. Tartu 2010, 248 p.

101. **Laura Herm.** Biochemistry of dopamine D_2 receptors and its association with motivated behaviour. Tartu 2010, 156 p.
102. **Terje Raudsepp.** Influence of dopant anions on the electrochemical properties of polypyrrole films. Tartu 2010, 112 p.
103. **Margus Marandi.** Electroformation of Polypyrrole Films: *In-situ* AFM and STM Study. Tartu 2011, 116 p.
104. **Kairi Kivirand.** Diamine oxidase-based biosensors: construction and working principles. Tartu, 2011, 140 p.
105. **Anneli Kruve.** Matrix effects in liquid-chromatography electrospray mass-spectrometry. Tartu, 2011, 156 p.
106. **Gary Urb.** Assessment of environmental impact of oil shale fly ash from PF and CFB combustion. Tartu, 2011, 108 p.
107. **Nikita Oskolkov.** A novel strategy for peptide-mediated cellular delivery and induction of endosomal escape. Tartu, 2011, 106 p.
108. **Dana Martin.** The QSPR/QSAR approach for the prediction of properties of fullerene derivatives. Tartu, 2011, 98 p.
109. **Säde Viirlaid.** Novel glutathione analogues and their antioxidant activity. Tartu, 2011, 106 p.
110. **Ülis Sõukand.** Simultaneous adsorption of Cd^{2+}, Ni^{2+}, and Pb^{2+} on peat. Tartu, 2011, 124 p.
111. **Lauri Lipping.** The acidity of strong and superstrong Brønsted acids, an outreach for the "limits of growth": a quantum chemical study. Tartu, 2011, 124 p.
112. **Heisi Kurig.** Electrical double-layer capacitors based on ionic liquids as electrolytes. Tartu, 2011, 146 p.
113. **Marje Kasari.** Bisubstrate luminescent probes, optical sensors and affinity adsorbents for measurement of active protein kinases in biological samples. Tartu, 2012, 126 p.
114. **Kalev Takkis.** Virtual screening of chemical databases for bioactive molecules. Tartu, 2012, 122 p.
115. **Ksenija Kisseljova**. Synthesis of aza-β^3-amino acid containing peptides and kinetic study of their phosphorylation by protein kinase A. Tartu, 2012, 104 p.
116. **Riin Rebane.** Advanced method development strategy for derivatization LC/ESI/MS. Tartu, 2012, 184 p.
117. **Vladislav Ivaništšev.** Double layer structure and adsorption kinetics of ions at metal electrodes in room temperature ionic liquids. Tartu, 2012, 128 p.
118. **Irja Helm.** High accuracy gravimetric Winkler method for determination of dissolved oxygen. Tartu, 2012, 139 p.
119. **Karin Kipper.** Fluoroalcohols as Components of LC-ESI-MS Eluents: Usage and Applications. Tartu, 2012, 164 p.
120. **Arno Ratas.** Energy storage and transfer in dosimetric luminescent materials. Tartu, 2012, 163 p.

121. **Reet Reinart-Okugbeni**. Assay systems for characterisation of subtype-selective binding and functional activity of ligands on dopamine receptors. Tartu, 2012, 159 p.
122. **Lauri Sikk.** Computational study of the Sonogashira cross-coupling reaction. Tartu, 2012, 81 p.
123. **Karita Raudkivi.** Neurochemical studies on inter-individual differences in affect-related behaviour of the laboratory rat. Tartu, 2012, 161 p.
124. **Indrek Saar.** Design of GalR2 subtype specific ligands: their role in depression-like behavior and feeding regulation. Tartu, 2013, 126 p.
125. **Ann Laheäär.** Electrochemical characterization of alkali metal salt based non-aqueous electrolytes for supercapacitors. Tartu, 2013, 127 p.
126. **Kerli Tõnurist.** Influence of electrospun separator materials properties on electrochemical performance of electrical double-layer capacitors. Tartu, 2013, 147 p.
127. **Kaija Põhako-Esko.** Novel organic and inorganic ionogels: preparation and characterization. Tartu, 2013, 124 p.
128. **Ivar Kruusenberg.** Electroreduction of oxygen on carbon nanomaterial-based catalysts. Tartu, 2013, 191 p.
129. **Sander Piiskop.** Kinetic effects of ultrasound in aqueous acetonitrile solutions. Tartu, 2013, 95 p.
130. **Ilona Faustova**. Regulatory role of L-type pyruvate kinase N-terminal domain. Tartu, 2013, 109 p.
131. **Kadi Tamm.** Synthesis and characterization of the micro-mesoporous anode materials and testing of the medium temperature solid oxide fuel cell single cells. Tartu, 2013, 138 p.
132. **Iva Bozhidarova Stoyanova-Slavova.** Validation of QSAR/QSPR for regulatory purposes. Tartu, 2013, 109 p.
133. **Vitali Grozovski**. Adsorption of organic molecules at single crystal electrodes studied by *in situ* STM method. Tartu, 2014, 146 p.
134. **Santa Veikšina**. Development of assay systems for characterisation of ligand binding properties to melanocortin 4 receptors. Tartu, 2014, 151 p.
135. **Jüri Liiv.** PVDF (polyvinylidene difluoride) as material for active element of twisting-ball displays. Tartu, 2014, 111 p.
136. **Kersti Vaarmets.** Electrochemical and physical characterization of pristine and activated molybdenum carbide-derived carbon electrodes for the oxygen electroreduction reaction. Tartu, 2014, 131 p.
137. **Lauri Tõntson**. Regulation of G-protein subtypes by receptors, guanine nucleotides and Mn^{2+}. Tartu, 2014, 105 p.
138. **Aiko Adamson.** Properties of amine-boranes and phosphorus analogues in the gas phase. Tartu, 2014, 78 p.
139. **Elo Kibena**. Electrochemical grafting of glassy carbon, gold, highly oriented pyrolytic graphite and chemical vapour deposition-grown graphene electrodes by diazonium reduction method. Tartu, 2014, 184 p.

140. **Teemu Näykki.** Novel Tools for Water Quality Monitoring – From Field to Laboratory. Tartu, 2014, 202 p.
141. **Karl Kaupmees.** Acidity and basicity in non-aqueous media: importance of solvent properties and purity. Tartu, 2014, 128 p.
142. **Oleg Lebedev**. Hydrazine polyanions: different strategies in the synthesis of heterocycles. Tartu, 2015, 118 p.
143. **Geven Piir.** Environmental risk assessment of chemicals using QSAR methods. Tartu, 2015, 123 p.
144. **Olga Mazina.** Development and application of the biosensor assay for measurements of cyclic adenosine monophosphate in studies of G protein-coupled receptor signalinga. Tartu, 2015, 116 p.
145. **Sandip Ashokrao Kadam.** Anion receptors: synthesis and accurate binding measurements. Tartu, 2015, 116 p.
146. **Indrek Tallo.** Synthesis and characterization of new micro-mesoporous carbide derived carbon materials for high energy and power density electrical double layer capacitors. Tartu, 2015, 148 p.
147. **Heiki Erikson.** Electrochemical reduction of oxygen on nanostructured palladium and gold catalysts. Tartu, 2015, 204 p.
148. **Erik Anderson.** *In situ* Scanning Tunnelling Microscopy studies of the interfacial structure between Bi(111) electrode and a room temperature ionic liquid. Tartu, 2015, 118 p.
149. **Girinath G. Pillai.** Computational Modelling of Diverse Chemical, Bio-chemical and Biomedical Properties. Tartu, 2015, 140 p.
150. **Piret Pikma.** Interfacial structure and adsorption of organic compounds at Cd(0001) and Sb(111) electrodes from ionic liquid and aqueous electrolytes: an *in situ* STM study. Tartu, 2015, 126 p.
151. **Ganesh babu Manoharan.** Combining chemical and genetic approaches for photoluminescence assays of protein kinases. Tartu, 2016, 126 p.